

A One-Dimensional Model of a Closed-Loop Refrigeration Test Block for Centrifugal Compressors

Paul D. Gessler
Marquette University

Recommended Citation

Gessler, Paul D., "A One-Dimensional Model of a Closed-Loop Refrigeration Test Block for Centrifugal Compressors" (2014). *Master's Theses (2009 -)*. Paper 243.
http://epublications.marquette.edu/theses_open/243

A ONE-DIMENSIONAL MODEL OF A CLOSED-LOOP
REFRIGERATION TEST BLOCK FOR
CENTRIFUGAL COMPRESSORS

by

Paul D. Gessler, B.S.

A Thesis submitted to the Faculty of the Graduate School,
Marquette University,
in Partial Fulfillment of the Requirements for
the Degree of Master of Science

Milwaukee, Wisconsin

May 2014

ABSTRACT
A ONE-DIMENSIONAL MODEL OF A CLOSED-LOOP
REFRIGERATION TEST BLOCK FOR
CENTRIFUGAL COMPRESSORS

Paul D. Gessler, B.S.

Marquette University, 2014

The increasingly competitive building equipment and control industry pushes manufacturers to continually improve the performance and efficiency of their products to develop and maintain a competitive edge. Compressor development is an expensive endeavor, but the cost and time required for testing can be minimized by developing a model of the compressor test block to predict its behavior with a given prototype compressor at specified operating conditions. This thesis presents a thermodynamic model of a hot gas bypass test block used to evaluate centrifugal compressor performance at a compressor development facility.

The test block uses cooling towers to reject the heat of compression to outdoor air, and experience has shown that the range of achievable compressor test conditions can be limited by outdoor air temperature and humidity, which affect the heat transfer rate. Therefore, one goal of the model development was to provide a means for evaluating the feasibility of tests at given outdoor air conditions. By incorporating models of the cooling towers into the test block model, test engineers now are able to predict the range of compressor suction and discharge conditions that can be tested under the current outdoor air conditions.

A second goal of the model was to assist in selecting the orifice plate used in the orifice flow meter that measures mass flow through the compressor. Engineers previously had to make an educated guess as to the best orifice plate size in advance of running the tests, but the model now identifies the orifice diameters that result in differential pressures within the desired range, minimizing the trial and error involved in testing.

The model assumes that the system operates at steady-state conditions and uses a compressor map to model expected prototype compressor performance. Therefore, this research focuses on the condenser and cooling tower models, which are the most important elements for predicting the impact of outdoor conditions on cycle performance. It is shown that the resulting model achieves agreement to within 2.5% of experimental data. The results for orifice differential pressure agree to within 0.35% of experimental data, providing a useful orifice selection routine.

ACKNOWLEDGMENTS

Paul D. Gessler, B.S.

This thesis and the associated modeling project would not have been possible without the support of many people. Specifically, I would like to thank my advisor, Dr. Margaret Mathison, for her unceasing encouragement, advice, and belief in my capabilities (even at times when I did not fully believe in them myself). Her technical knowledge in the subject area was a great asset to the project, to be sure. But of equal or greater importance to me was her constant patience and willingness to provide advice, keeping me grounded through this entire process.

I would also like to thank the other members of my committee: Dr. Anthony Bowman provided valuable advice on EES features, helped me through my first experiences as a teaching assistant, and took time to give me a tour of the department when I was first considering Marquette for graduate school. Mr. John Trevino, Jr. served as my main technical contact at JCI for the project. I thank him for taking time to answer my questions or pointing me towards people with the answers, hosting and helping me during my trip to York during November 2012, and for providing valuable feedback on the usability of the model in everyday work. Finally, I thank Dr. Robert Turney for serving as my mentor during my internship at JCI, showing me the benefits of model-based design processes and automated testing approaches, and continuing his commitment to my education through serving on my committee.

While not formally members of my committee, two more engineers merit special recognition here. I would like to acknowledge Mr. Brett Lenhardt and Mr. Steven Sommer. Mr. Lenhardt's dynamic modeling work at JCI inspired my interest in modeling specifically applied to thermal and fluid systems. He also provided feedback as the project was defined and progressed. Mr. Sommer provided valuable comments on my thesis as well as crucial insight during project meetings. He also facilitated my November 2012 trip to York, PA, during which I learned about the equipment modeled here and collected experimental data essential to the validation of the model.

Special thanks to the faculty and staff in the Department of Mechanical Engineering, the Graduate School, and Marquette University as a whole for their funding through my teaching assistantship and other support. Your efforts and support made my graduate education possible. To my students: your dedication and perseverance inspired me during my time at Marquette. I also thank my fiancée, Elise, my parents, Timothy and Shelley, and the rest of my family for their never-ending support, encouragement, understanding, and love.

Soli Deo gloria.

TABLE OF CONTENTS

ACKNOWLEDGMENTS	i
LIST OF TABLES	v
LIST OF FIGURES	vi
LIST OF CODE LISTINGS	viii
LIST OF SYMBOLS	ix
1 INTRODUCTION	1
1.1 Background	3
1.2 Motivation	4
1.3 Objectives	5
1.4 Requirements and Constraints	6
1.5 Organization	7
2 LITERATURE REVIEW	8
2.1 General Compressor Testing	8
2.1.1 Compressor Testing Methodology—ASME PTC 10	8
2.1.2 Compressor Performance Metrics	9
2.2 Existing Component Thermodynamic Models	10
2.2.1 Flow Measurement Orifice	10
2.2.2 Condenser	10
2.2.3 Cooling Tower	11
2.2.4 Minor Components	11

2.3	Test Block Design and Construction	12
2.4	Summary	12
3	THEORETICAL MODEL DEVELOPMENT	13
3.1	General Balance Equations	13
3.2	Compressor	15
3.3	Orifice Flow Meter	18
3.4	Flow Split	20
3.5	Condenser	21
3.6	Cooling Tower	23
3.7	Expansion Devices	25
3.8	Mixing Chamber	25
4	SOLUTION METHODOLOGY	27
4.1	Implementation Structure	28
4.2	Complete Cycle Program	28
4.3	Orifice Selection Program	29
5	RESULTS AND DISCUSSION	35
5.1	Comparison of Experimental and Model Results	36
5.1.1	Compressor Module	36
5.1.2	Orifice Module	38
5.1.3	Condenser Module	41
5.1.4	Cooling Tower Module	42
5.2	Sensitivity Analysis	43

6	CONCLUSIONS AND RECOMMENDATIONS	47
6.1	Conclusions	47
6.2	Recommendations	48
	BIBLIOGRAPHY	50
	APPENDICES	52
A	ENGINEERING EQUATION SOLVER (EES) CODE LISTING	52
B	SAMPLE VALIDATION DATA AND RESULTS	63

LIST OF TABLES

4.1	Orifice numbering and diameter data for the modeled test block (Graham, 2006). This table corresponds to the information stored in the EES lookup table 'OrificeData'	30
5.1	Sensitivity analysis results for the compressor Reynolds number, Re . The reference Reynolds number for this condition is $Re = 2.591 \times 10^6$	44
5.2	Sensitivity analysis results for the orifice Reynolds number, Re . The reference Reynolds number for this condition is $Re = 7.891 \times 10^6$	45
5.3	Sensitivity analysis results for the condenser water mass flow rate, \dot{m}_w . The reference water flow rate for this condition is $\dot{m}_w = 6768 \text{ lbm min}^{-1}$	46
B.1	Sample validation results. Protected information is removed from the table and denoted with 'JCI Proprietary'. Percent differences for temperatures are calculated on an absolute basis.	64

LIST OF FIGURES

1.1	Comparison of idealized temperature-entropy (T - s) diagrams.	3
(a)	Vapor-compression refrigeration cycle.	3
(b)	Hot gas bypass test block cycle.	3
1.2	Simplified schematic of the 1500 hp gas test block facility.	5
3.1	Typical compressor map, showing flow and head axes, speed lines, and efficiency islands. The operating region for the compressor is the region bounded by the surge and choke lines.	15
4.1	Engineering Equation Solver (EES) Diagram Window for the complete cycle program. User inputs are boxed numbers, while program outputs are displayed without boxes.	29
4.2	Flowchart for orifice selection procedure. The inner loop is over the orifices listed in Table 4.1 and the outer loop is over the user-specified range of flow coefficients.	31
4.3	Engineering Equation Solver (EES) Diagram Window for the orifice selection program. User inputs are boxed numbers, while program outputs are displayed without boxes.	32
4.4	Typical orifice selection program results. The axis limits correspond to the 10 inH ₂ O to 990 inH ₂ O acceptable measurement range.	33
4.5	Orifice selection program results showing choked flow for orifices 3–14. For these conditions, only orifice 2 is acceptable over the entire range of flow coefficients.	34
5.1	Compressor discharge pressure parity plot.	37
5.2	Compressor discharge temperature parity plot.	37
5.3	Compressor Reynolds number parity plot.	38
5.4	Compressor gas horsepower parity plot.	39
5.5	Orifice temperature parity plot.	40

5.6	Orifice differential pressure parity plot.	40
5.7	Condenser pressure parity plot.	41
5.8	Condenser refrigerant liquid temperature parity plot.	42
5.9	Average condenser water temperature parity plot.	43

LIST OF CODE LISTINGS

A.1	Main EES program code.	52
A.2	General helper functions.	54
A.3	Helper functions specific to the compressor and orifice modules.	55
A.4	Compressor module of EES implementation.	56
A.5	Orifice module of EES implementation.	57
A.6	Flow split module of EES implementation.	58
A.7	Condenser module of EES implementation.	59
A.8	Expansion device module of EES implementation.	60
A.9	Cooling tower module of EES implementation.	61

LIST OF SYMBOLS

Symbol	Description	Units
a	Acoustic (sonic) velocity	ft min ⁻¹
A	Area	ft ² , in ²
b	Impeller tip width	ft, in
C	Orifice coefficient of discharge	–
c_p, c_v	Specific heats, constant pressure and volume, respectively	Btu lbm ⁻¹ R ⁻¹
c_s	Saturation specific heat	Btu lbm ⁻¹ R ⁻¹
D	Diameter	ft, in
d	Orifice diameter	ft, in
e	Specific energy, $e = u + ke + pe$	Btu lbm ⁻¹
g	Gravitational acceleration, $g = 115\,826\text{ ft min}^{-2}$	ft min ⁻²
g_c	Gravitational proportionality constant, $g_c = 115\,826\text{ lbm ft lbf}^{-1}\text{ min}^{-2}$	lbm ft lbf ⁻¹ min ⁻²
h	Specific enthalpy, $h = u + pv$	Btu lbm ⁻¹
h°	Specific methalpy, $h^\circ = h + ke + pe$	Btu lbm ⁻¹
ke	Specific kinetic energy, $ke = \mathcal{V}^2/2$	Btu lbm ⁻¹
$K_{(\)}$	Flow coefficients for orifice correlations; refer to Section 3.3 for details	–
m	Mass	lbm
Ma	Machine Mach number, \mathcal{V}_{tip}/a	–
NTU	Number of transfer units	–
p	Pressure	psia, psig, psid
pe	Specific potential energy, $pe = gz$	Btu lbm ⁻¹

Q	Heat transfer	Btu
$Re_{(\)}$	Reynolds number based on characteristic length ($\)$, $Re_{(\)} = \rho \mathcal{V}(\) / \mu$	-
s	Specific entropy	Btu lbm ⁻¹ R ⁻¹
T	Temperature	°F, R
t	Time	min
u	Specific internal energy	Btu lbm ⁻¹
v	Specific volume	ft ³ lbm ⁻¹
\mathcal{V}	Velocity magnitude	ft min ⁻¹
W	Work transfer	Btu
X	Flow ratio, $X = \min(1, \Theta / \Theta_{\text{peak}})$	-
x	Quality	-
Y	Expansion factor	-
z	Elevation	ft
*	Unless otherwise noted, symbols for extensive properties are the uppercase variants of symbols used for the corresponding specific (intensive) properties.	

Greek Symbols

α	Correction factor for orifice correlations; refer to Section 3.3 for details	-
β	Ratio of orifice diameter to pipe diameter, $\beta = d / D$	-
ϵ	Heat exchanger (or cooling tower) effectiveness, $\dot{Q} / \dot{Q}_{\text{max}}$	-
η	Efficiency	-
γ	Ratio of specific heats, $\gamma = c_p / c_v$	-
μ	Dynamic viscosity	lbf min ft ⁻²
Ω	Isentropic head coefficient, $g_c \Delta h_s / a^2$	-

ω	Absolute humidity ratio	$\text{lbm}_w/\text{lbm}_a$
ρ	Density, $1/v$	lbm ft^{-3}
Θ	Flow coefficient, \dot{V}/aD^2	–

Subscripts

a	Air-water vapor mixture
CV	Control volume
i	Inlet conditions
o	Outlet conditions
r	Refrigerant
s	Saturated
sh	Superheat
w	Water
i	The i th component/element of a mixture/series
s	Isentropic

Conventions

$\Delta()$	Change in quantity; for example, final – initial or outlet – inlet	[]
$\dot{()}$	Quantity per unit time or rate, $d()/dt$	[]/min
$\langle \rangle$	Singularity function notation, $\max(0, \langle \rangle)$	[]

Abbreviations

ASME	American Society of Mechanical Engineers
BAC	Baltimore Aircoil Company
CFD	Computational Fluid Dynamics
EES	Engineering Equation Solver

HGBP	Hot Gas Bypass
HVAC	Heating, Ventilating, and Air Conditioning
JCI	Johnson Controls, Inc.
PTC	Performance Test Code
RTD	Resistance Temperature Detectors

CHAPTER 1

INTRODUCTION

The increasingly competitive building equipment and control industry pushes manufacturers to devote more resources each year to research and development, continually improving the performance and efficiency of their products to develop and maintain a competitive edge. The design of centrifugal compressors is no exception to this trend, since these compressors are used in many power-intensive applications, including water-cooled chillers in large commercial and industrial buildings. The compressor transfers energy from the source (often a shaft driven by an electric motor) into the refrigeration cycle, and is thus a scrutinized component of the overall design.

Compressor development is an expensive endeavor because of prototyping and testing costs. The design of a new compressor requires at least one prototype to be constructed, which is then subjected to a series of industry-standard performance tests to quantify the improvements in the new design. This adds cost and development time to an already expensive process. For example, the costs for one week of testing can approach \$10 000 (Sommer, 2013). The requirement of physical performance tests should not be disputed, since the resulting ratings are used by potential customers to compare offerings from different manufacturers. Additionally, all models are approximations of the real system and cannot completely capture the behavior of the physical system.

Nevertheless, minimizing testing time has a large impact on costs and time to market. A test block model based on first principles has the potential to reduce the testing time and thus decrease costs by assisting the test engineer in defining an optimized test plan built around test block capabilities at the expected ambient conditions. Furthermore, the downtime for changing flow measurement orifices can be minimized by providing a means to choose the best orifice diameter for a given range of test flow rates.

With these considerations in mind, the overall goal of this research is to create a thermodynamic model to simulate the 1500 hp gas block compressor testing equipment used by Johnson Controls, Inc. (JCI) at their facility in York, Pennsylvania. This equipment uses a hot gas bypass (HGBP) cycle to simulate the compressor operating conditions of the actual refrigeration cycle without requiring an evaporator or associated cooling load. The primary refrigerant used in this system is R-134a, but the equipment allows for a wide variety of refrigerants to be used, as should the thermodynamic model.

The model will use the design conditions of the new compressor (mass flow, pressure head, shaft speed, and isentropic/map efficiency) to determine the test block setup (flow measurement orifice size and cooling tower fan speed) required to conduct tests at given ambient conditions. The current testing process requires some trial and error to find a suitable test block setup for a new compressor. The thermodynamic model aims to quickly provide reasonably accurate initial estimates of the orifice diameter (based on differential pressure) and cooling tower fan speed (based on condenser heat transfer) required to test a new compressor at specified outdoor air conditions (temperature, barometric pressure, and relative humidity). Therefore, the testing time is reduced by eliminating (or at least minimizing) the trial and error phase of the testing process.

The equipment and configuration of a typical hot gas bypass test block cycle is described thoroughly in existing literature, primarily in work by McGovern (1984), Dirlea, Hannay, and Lebrun (1996), and Sahs and Mould (1956). Thermodynamic models of the individual components in the test block cycle exist, are well-established, and are used frequently in the thermal and fluid sciences. The novelty of this thesis is not derived from breakthroughs in the modeling theory surrounding the components, but rather from an integration of existing models into a holistic tool at an appropriate level for use in industry applications. Its significance may be measured by the impact on the daily workflow of test engineers in the compressor development group.

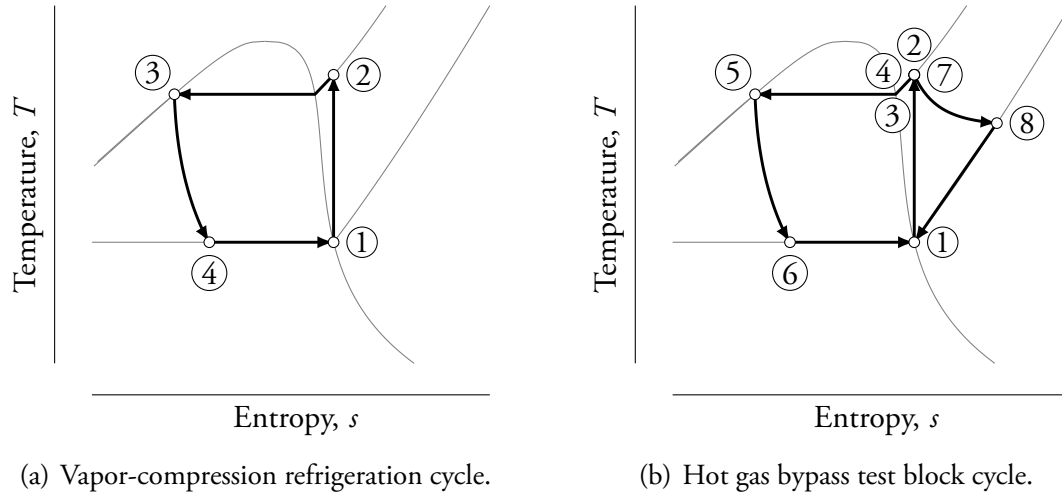


Figure 1.1: Comparison of idealized temperature-entropy ($T-s$) diagrams.

1.1 Background

A preferred method of evaluating compressor performance is to test the compressor on a closed-loop gas test block using the design process fluid (refrigerant) at design flow conditions. While the equipment can be expensive to construct, operate, and maintain, the gas test block makes isolating the compression portion of the refrigeration cycle easier. The basic premise of the gas test block cycle is that the cycle can maintain conditions at the compressor inlet similar to those experienced in a traditional vapor-compression refrigeration cycle, while the conditions at other points in the cycle need not follow the traditional refrigeration cycle arrangement. Temperature-entropy ($T-s$) diagrams for the typical vapor-compression refrigeration cycle and an idealized gas block test cycle are shown in Fig. 1.1, with process 1–2 representing the ideal, isentropic compression process for both cycles.

There are energy savings associated with using the gas test block instead of the chiller refrigeration cycle. Process 4–1 of the traditional refrigeration cycle of Fig. 1.1(a) is the result of heat transfer into the evaporator, which is the building cooling load or refrigeration effect. In a chiller test block situation, this load is simulated by mixing water from the condenser and evaporator loops. In the gas block test cycle, no water loop is required for this process, state 1

being reestablished instead by mixing saturated liquid-vapor mixture (state 6) with a superheated vapor separated from the discharge stream and throttled to the cycle's low pressure (state 8). The conditions at state 1 are controlled by adjusting the discharge flow split that occurs near state 2 of Fig. 1.1(b). In addition to eliminating one water loop from the system, the condenser heat transfer—process 4–5 of Fig. 1.1(b)—is also reduced because only a portion of the refrigerant flow must be condensed.

A primary benefit of this arrangement is that the gas block is more versatile than a traditional refrigeration cycle used in a chiller. The gas block can handle a wide variety of test gases (refrigerants) and their associated operating pressures and cooling loads, while a chiller may require different heat exchangers or piping to operate with certain refrigerants at a full range of operating conditions. Additionally, the gas test block provides better locations for instrumentation and conforms to industry-standard test codes (for example, ASME PTC 10) outlining proven and well-established data analysis and results reporting methods. For example, the test code specifies straight sections of suction pipe and/or flow straighteners to produce near-axial flow, while the compact piping arrangement on a chiller causes large deviations from axial flow. Using a gas test block provides an even basis of comparison for compressors independent of the chiller design. A simplified schematic of the test block layout is shown in Fig. 1.2, with state numbering corresponding to Fig. 1.1(b).

1.2 Motivation

As discussed in the opening of Chapter 1, the numerical model of the test block will reduce the time required during physical testing of new compressor designs by helping engineers choose an appropriate test setup for a particular compressor. The parameters of the test setup predicted by the model include the flow measurement orifice diameter and the cooling tower fan speeds.

Additionally, the model will check whether or not a set of test conditions can be achieved at specified outdoor air conditions. These air conditions limit the performance of the

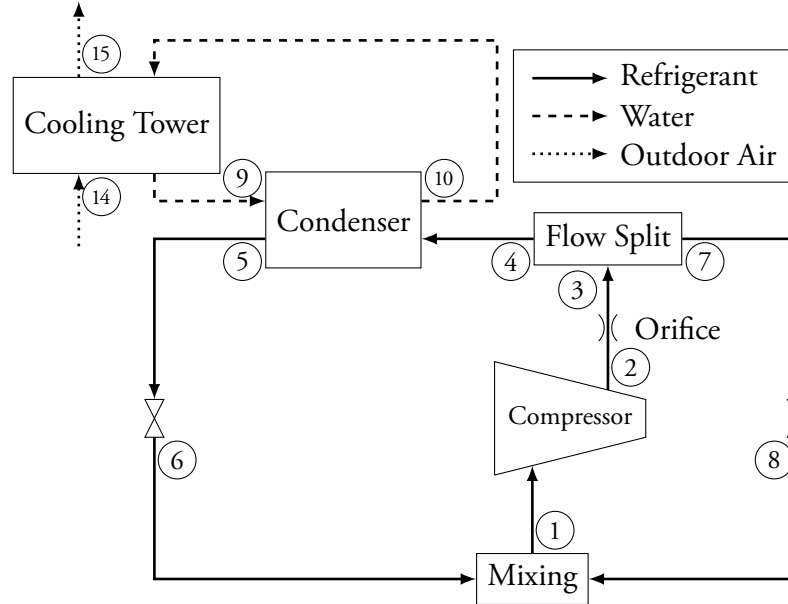


Figure 1.2: Simplified schematic of the 1500 hp gas test block facility.

cooling towers and may preclude certain compressor tests. This prediction could prevent the loss of time and resources required to set up a compressor test for conditions that are not feasible at the current outside temperature and humidity.

Finally, JCI has expressed interest in building an automated test block in the future. If desired, the present model could be adapted for use in a model-based controls design workflow to expedite and enhance the control system design process. This is a long-term motivation and is secondary to the test time reduction and limiting conditions motivations.

1.3 Objectives

The overall goal of this research is to develop a one-dimensional, steady-flow thermodynamic model representing the 1500 hp gas test block at JCI's York, PA facility. The numerical model will be used in conjunction with compressor maps and/or computational fluid dynamics (CFD) models of the compressors to quantitatively predict the performance of new compressor designs on the test block. To accomplish the overall goal and satisfy the needs of JCI (Iancu, 2012), the model must

- compute the power requirements for the prime mover of the test block,
- choose the orifice diameter that results in the smallest error in measured flow rate over the desired range of operating conditions, and
- report the limits of the test block operating conditions for a given compressor design, test block control settings, and ambient air conditions.

1.4 Requirements and Constraints

The compressor test block model should be one-dimensional and steady-flow in nature; that is, the flow conditions at a cross section of flow are treated as spatially uniform and constant over time. Modeling is conducted on a macroscopic level, neglecting the effects of property gradients within the flow, such as viscous and thermal boundary layers. Modeling such detailed phenomena would complicate the model and would not significantly improve the predictions requested by JCI listed in Section 1.3.

The numerical model must be easy for engineers in the compressor engineering group at JCI to use and update and should minimize dependencies on licensed software for better portability. The software tools generally available to the compressor engineering group are Engineering Equation Solver (EES) and MATLAB/Simulink. Engineering Equation Solver was chosen since MATLAB/Simulink is more suited to dynamic models, the engineers at York are more familiar with EES, and EES has built-in thermophysical property relations while MATLAB/Simulink requires interfacing with an external library.

The execution time of the model is a primary concern of JCI's compressor engineers, and should be less than one minute for each individual compressor test. The accuracy of the model is another critical requirement. Output variables concerning the compressor and flow measurement orifice must not deviate from experimental results by more than 5%. At other areas in the cycle, such as at the condenser and cooling tower, a relaxed maximum deviation of 10% is required. This is justified by the inherent complexities in modeling the heat transfer in both the condenser and cooling tower and the relatively small impact on the desired outputs.

1.5 Organization

This thesis documents the creation of the one-dimensional, steady-flow test block model for use by compressor development and test engineers at JCI's York, PA location. Chapter 1 has introduced the work, its motivation and objectives, and provided an overview of the assumptions and form of the project. Chapter 2 summarizes the current state of the art compressor testing and modeling techniques and other reference materials used in developing and implementing the model. Chapter 3 presents the mathematical formulation of the model and its inherent engineering assumptions. Chapter 4 documents the implementation of the numerical model, including numerical solution techniques and user interface considerations.

Chapter 5 presents the predictions of the model for a variety of compressor designs and operating points. These predictions are compared to corresponding experimental data from physical tests to validate the model predictions. A discussion of the validation results is included, highlighting the strengths and weaknesses of the numerical model. Chapter 6 summarizes the research work and provides recommendations to users of the model and future maintainers.

Appendix A contains code listings of the EES implementation for the compressor gas test block model described in Chapter 4. Brief explanations of the code are included. Appendix B presents a sample set of validation results. This includes a set of experimental data from the test block data analysis program and the corresponding model outputs. The validation effort is described in detail in Chapter 5.

CHAPTER 2

LITERATURE REVIEW

As discussed in Chapter 1, thermodynamic models of each component in the hot gas bypass test cycle have already been created and are widely used. This literature review surveys the existing test methods and models and summarizes information about the JCI test block cycle, including equipment details. A general description of each source is contained here, while any mathematical models used are presented (with citations) in the complete model development of Chapter 3.

2.1 General Compressor Testing

One component of the research effort was to study different methods of testing compressors. Therefore, this section provides information regarding compressor performance metrics and testing methods commonly used in the HVAC industry. The research was done to better understand the testing methodology, the data collected during a typical test, and the expectations for a mathematical model of the test block refrigeration cycle.

2.1.1 Compressor Testing Methodology—ASME PTC 10

The ASME PTC 10-1972 standard (Gerber, 1998) prescribes test conditions, procedures, and measurement locations for a compressor test. This allows different manufacturers' test results to be compared. The standard also presents dimensionless coefficients used by different industries to characterize the operating point of the compressor with associated conversions. The relevant coefficients are described in greater detail as part of the compressor model development in Section 3.2. These coefficients serve as inputs to the thermodynamic model that fully characterize the performance of the compressor. Because the compressor operating point constrains many variables in the model, these coefficients are critical to the model's performance.

Significant portions of PTC 10 focus on multistage compressor testing and sideload calculations. These are not needed for the present modeling effort, since the vast majority of recent compressor tests conducted on the 1500 hp gas test block use single-stage compressor setups (Trevino, 2012).

Finally, ASME PTC 10 contains several sets of sample calculations which are of use in verifying the implementation of the model, particularly the calculation of the prime mover power requirements. These calculations are similar in form to those used in the existing compressor test block data acquisition program and the compressor module of the present thermodynamic model.

2.1.2 Compressor Performance Metrics

Although ASME PTC 10 prescribes many parts of the test methodology, it is also important to understand other recommendations for compressor testing. Wilcox (2007) advocates the use of ASME PTC 10 (Section 2.1.1) and lists suction and discharge pressures, suction and discharge temperatures, mass flow rate, fluid (refrigerant) composition, rotational speed, and driver load as critical field data for any compressor test. These critical field data also appear as inputs or outputs of the thermodynamic model of the compressor, presented in Section 3.2.

Furthermore, Wilcox outlines some general guidelines for instrumentation on the test block to ensure representative data. He notes that pressure and temperature sensors should be located at least 10 pipe diameters from potential disturbances or obstructions such as tees or elbows. All sensors should be calibrated prior to the test run, and data should only be collected at steady-state conditions. For a typical compressor test, Wilcox defines steady-state conditions to be achieved once the discharge temperature remains constant (within sensing accuracy) over a 15 min interval. According to Wilcox, resistance temperature detectors (RTDs) should be used instead of thermocouples wherever possible for improved accuracy. Finally, he stresses the importance of recording test data at several different operating points to allow recognition of a

bad measurement in any one set of data. All of these guidelines are met by the instrumentation and testing procedures in use on the 1500 hp gas test block at JCI. This ensures that validation data provide a good representation of the actual operation of the system.

2.2 Existing Component Thermodynamic Models

The 1500 hp gas test block contains a number of components which must be modeled. The compressor is not directly modeled in this work, which instead uses external compressor maps or other means to specify the discharge conditions given a set of suction conditions as discussed in Sections 2.1.1 and 3.2. The flow measurement orifice, hot gas bypass (HGBP) flow split, condenser, cooling towers, throttling expansion devices, and a mixing chamber must be modeled. This section summarizes a number of texts and papers that were consulted to model these devices.

2.2.1 Flow Measurement Orifice

The flow measurement orifice is modeled according to correlations presented in ASME PTC 19.5 (American Society of Mechanical Engineers, 1972) and following the general form of Munson, Young, Okiishi, and Huebsch (2009). The ASME PTC 19.5 standard presents relationships between the differential pressure across the orifice and the flow rate, as shown in Section 3.3. Compressible effects are included since the refrigerant will be in a superheated vapor state at the orifice. According to Trevino (2012) and J.N.O. (1984), flange taps are used on the test block, so the correlations in ASME PTC 19.5 for flange tap pressure measurements are used.

2.2.2 Condenser

Incropera, DeWitt, Bergman, and Lavine (2007), Incropera and DeWitt (1985), and Kays and London (1984) developed equations describing the performance of the condenser, which in this case is a shell-and-tube unit. The NTU-effectiveness method is used to calculate

the heat transfer rate in terms of inlet and outlet temperatures since internal temperature measurements are not available. Engineering drawings from JCI (J.N.O., 1983) and a technical manual for the condenser (York Division, Borg-Warner Corporation, n.d.) were used, along with experimental data, to determine the effectiveness and number of transfer units for the condenser.

2.2.3 Cooling Tower

Braun, Klein, and Mitchell (1989) and Mitchell and Braun (2013) developed equations for modeling cooling towers using an effectiveness approach analogous to the heat exchanger model. This is useful as it avoids iteration wherever possible and does not require detailed cooling tower data. An example useful for verification of the cooling tower model is presented by Mitchell and Braun (2013). The model requires two characteristic performance parameters, which affect the number of transfer units (NTU) of the cooling tower. Therefore, a linear regression process is performed on experimental data from the Baltimore Aircoil Company (BAC) cooling towers (Baltimore Aircoil Company, Inc., 2001) to determine these parameters. Braun et al. (1989) outlined this process and provided several values for typical cooling towers. These parameters are discussed in Section 3.6. Qureshi and Zubair (2006) extended the model to include fill fouling. The effect of fill fouling is not included currently, but could be added in the future if desired.

2.2.4 Minor Components

The flow split, expansion devices, and mixing chamber are modeled using basic extensive property balances (mass and energy) as detailed in undergraduate thermodynamics texts such as Çengel and Boles (2011). The equations are developed from the general balance equations in Sections 3.4, 3.7, and 3.8.

2.3 Test Block Design and Construction

In addition to the York documentation already cited, further details regarding the test facility are found in the Applied Systems Operating Limits report (Graham, 2006). This includes pipe diameters, orifice diameters, and operating instructions. The condenser water pump is a fixed-speed unit, Aurora Type 410, size $6 \times 8 \times 15$, with pump curves given by Aurora Pentair Water (2007).

The US Patent by Sahs and Mould (Apparatus for Testing Refrigeration Compressors, 1956), Dirlea et al. (1996), and McGovern (1984) describe the general configuration of the cycle, and illustrate how the different components interact with one another. However, no holistic modeling effort is attempted in any of these sources.

2.4 Summary

To the best of the author's knowledge, a complete model of the hot gas bypass test block cycle is a novel undertaking. The completion of this model will have significant impact on the testing process used every day by test engineers at JCI (Sommer, 2013). The survey of literature contained in Chapter 2 provides the theoretical basis for each component-level model in the complete cycle. Chapter 3 will discuss each component model in greater detail.

CHAPTER 3

THEORETICAL MODEL DEVELOPMENT

This chapter presents the development of the equations used to model the compressor test block from first principles. Section 3.1 contains the general mass and energy balance equations, to which the appropriate assumptions for each device in the cycle are applied to produce the device-specific equations, as detailed in Sections 3.2 to 3.8. Subscripts i and o are used to indicate the inlet and outlet states of the device, respectively.

3.1 General Balance Equations

The rate forms of the balance equations are used throughout the model. This section lists the mass and energy balances in their most general form (Çengel & Boles, 2011), so that engineering assumptions may be applied on a per-device basis.

The general mass balance is obtained by applying conservation of mass to the control volume. This process yields

$$\frac{dm_{CV}}{dt} = \sum_{\text{inlets}} \dot{m}_i - \sum_{\text{outlets}} \dot{m}_o, \quad (3.1)$$

where the summations account for any number of inlets and outlets to the device.

Equation (3.1) includes only transport terms since mass production is always identically zero (neglecting nuclear processes). This result is applied to each device in the cycle, with the appropriate number of inputs and outputs.

Similarly, the general energy balance is obtained by writing an extensive property balance over the control volume. By the first law of thermodynamics, energy production is identically zero (again, neglecting nuclear processes), so only transport terms remain in the equation. However, heat transfer and work transfer interactions, and kinetic and potential energy changes can change the energy of the control volume in addition to the transport terms,

so

$$\frac{dE_{CV}}{dt} = \dot{Q} - \dot{W} + \sum_{\text{inlets}} (\dot{m} h^\circ)_i - \sum_{\text{outlets}} (\dot{m} h^\circ)_o, \quad (3.2)$$

where the *methalpy*, $h^\circ = h + ke + pe$, is a convenient way to account for the enthalpy, h , and kinetic and potential energy effects if required. The kinetic energy can be calculated as

$$ke = \mathcal{V}^2/2, \quad (3.3)$$

where the average velocity \mathcal{V} can be calculated using $\dot{m} = \rho \mathcal{V} A$. The potential energy can be calculated as

$$pe = g z, \quad (3.4)$$

where g is the gravitational acceleration and z is the elevation of the inlet/outlet.

Equation (3.2) shows the standard sign convention used throughout this thesis; that is, heat transfer *into* the system is considered positive, while work transfer *out of* the system is considered positive. Equations (3.1) and (3.2) form the basic equations to which engineering assumptions are applied in Sections 3.2 to 3.8. Assumptions common to each device in the cycle are that

1. the steady-flow condition eliminates both time derivatives dm_{CV}/dt and dE_{CV}/dt ,
2. changes in potential energy are neglected, so $\Delta pe = 0$, and
3. changes in kinetic energy are neglected, so $\Delta ke = 0$.

As a consequence of assumptions 2 and 3, the methalpy notation reduces to the more familiar enthalpy form, and assumption 1 means that the left-hand sides of Eqs. (3.1) and (3.2) both become zero:

$$0 = \sum_{\text{inlets}} \dot{m}_i - \sum_{\text{outlets}} \dot{m}_o, \quad (3.5)$$

$$0 = \dot{Q} - \dot{W} + \sum_{\text{inlets}} (\dot{m} h)_i - \sum_{\text{outlets}} (\dot{m} h)_o. \quad (3.6)$$

Eqs. (3.5) and (3.6) are used as the basis for all component models in Sections 3.2 to 3.8.

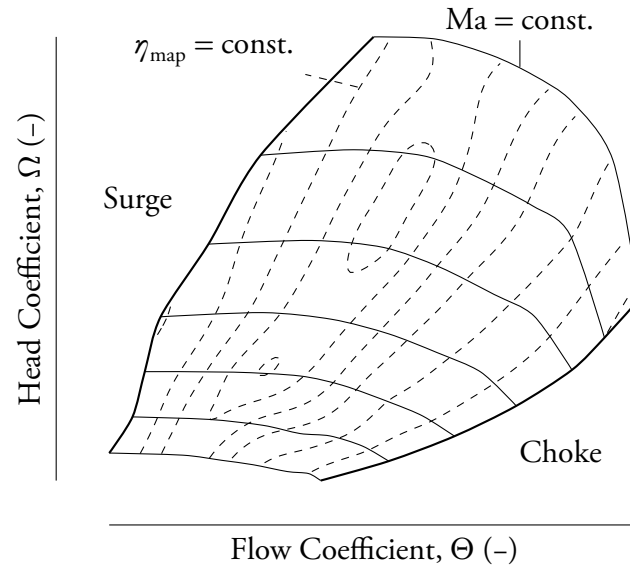


Figure 3.1: Typical compressor map, showing flow and head axes, speed lines, and efficiency islands. The operating region for the compressor is the region bounded by the surge and choke lines.

3.2 Compressor

Detailed modeling of the compressor is complex and worthy of a dissertation in its own right. To make matters worse, the model should make reasonable predictions of a compressor test for *any* compressor, whether already prototyped or in the early stages of development. Fortunately, detailed compressor models for predicting compressor performance are not required for the purposes of test block modeling. Instead, the performance of the compressor is calculated by the model using data from compressor maps. An example of a typical compressor map is shown in Fig. 3.1. These compressor maps are developed by JCI either experimentally for existing compressors or numerically—using other compressor design tools, from basic one-dimensional methodologies to full three-dimensional CFD—for new compressor designs.

A user of the model can select an operating point on the compressor map, and with specification of the suction (inlet) conditions, the discharge (outlet) state of the compressor is fixed. The compressor maps use the dimensionless coefficients of flow, head, velocity, and efficiency (Θ , Ω , Ma , and η_s , respectively) to generalize machine characteristics. The flow

coefficient, Θ , (Trevino, 2012) is given by

$$\Theta = \frac{\dot{V}}{aD^2}, \quad (3.7)$$

where \dot{V} is the volumetric flow rate, a is the acoustic (sonic) velocity at total suction conditions, and D is the impeller tip diameter. The head coefficient, Ω , (Trevino, 2012) is given by

$$\Omega = \frac{g_c \Delta h_s}{a^2}, \quad (3.8)$$

where g_c is the gravitational proportionality constant, Δh_s is the specific enthalpy change for an isentropic compression process, and a is, again, the acoustic velocity at total suction conditions.

The Machine Mach number, Ma , is

$$\text{Ma} = \frac{\mathcal{V}_{\text{tip}}}{a}, \quad (3.9)$$

where \mathcal{V}_{tip} is the impeller tip velocity and a is the acoustic velocity at total inlet (suction) conditions (Trevino, 2012). The third and final compressor performance characteristic gleaned from the compressor map is the isentropic efficiency, η_s , which quantifies the deviation of the real compression process from an isentropic (adiabatic and reversible) compression process. The isentropic efficiency (Çengel & Boles, 2011) is defined as

$$\eta_s = \frac{h_{os} - h_i}{h_o - h_i}, \quad (3.10)$$

where h_{os} is the discharge enthalpy for an isentropic compression process, h_i is the suction enthalpy, and h_o is the actual discharge enthalpy.

While the model uses isentropic efficiency, η_s , the efficiency islands on standard compressor maps plot a corrected efficiency, η_{map} , which includes a correction for the Reynolds number at the given operating point. To convert the corrected map efficiency into isentropic efficiency (Kauffman & Sommer, 2006), the transformation

$$\eta_s = \eta_{\text{map}} + X(1 - \eta_{\text{peak}}) \left(1 - \left(\frac{10^6}{\text{Re}_b} \right)^{0.1} \right) \quad (3.11)$$

is used. In Eq. (3.11), the flow ratio, X , is given by

$$X = \begin{cases} \Theta/\Theta_{\text{peak}} & \text{if } \Theta/\Theta_{\text{peak}} < 1 \\ 1 & \text{if } \Theta/\Theta_{\text{peak}} \geq 1 \end{cases}, \quad (3.12)$$

where Θ_{peak} is the flow coefficient corresponding to the point of maximum map efficiency.

Additionally, η_{peak} is the maximum map efficiency and Re_b is the Reynolds number based on impeller tip width b ; that is,

$$\text{Re}_b = \frac{\rho \mathcal{V} b}{\mu}, \quad (3.13)$$

with fluid properties evaluated at total suction conditions.

The four map parameters for the desired operating point (Θ , Ω , Ma , and η_{map}), specified suction conditions (T_i and p_i), and machine characteristics (D , b , Θ_{peak} , and η_{peak}) allow the model to compute the discharge conditions (T_o and p_o) and mass flow rate \dot{m} . Once the inlet and outlet states at the compressor are known, the mass and energy balances can be revisited. From Eqs. (3.5) and (3.6) and assuming that the compressor can be modeled as a single-input, single-output (SISO) device (no leakage assumption), the balance equations become

$$\text{Mass:} \quad 0 = \dot{m}_i - \dot{m}_o \quad (3.14)$$

$$\text{Energy:} \quad 0 = \dot{Q} - \dot{W} + (\dot{m}h)_i - (\dot{m}h)_o. \quad (3.15)$$

Equation (3.14) simply means that the mass flow entering the compressor is equal to that leaving the compressor. The mass flow rate is known from the calculation procedure with the compressor map parameters. Finally, assuming that the compressor is well-insulated, $\dot{Q} = 0$, leaves \dot{W} as the sole remaining unknown in Eq. (3.15). This value is one of the required outputs of the model.

The value calculated for \dot{W} in the compressor is known as the *gas horsepower* because it represents the power input directly to the gas. The actual power requirements of the prime

mover are slightly larger as a result of mechanical inefficiencies in the speed-increasing gearbox and compressor itself. These losses are modeled assuming the form

$$\dot{W}_{\text{gas}} = \eta_{\text{mech}} \dot{W}_{\text{mech}}, \quad (3.16)$$

with an empirical mechanical efficiency factor η_{mech} which is discussed further in Chapter 4.

3.3 Orifice Flow Meter

American Society of Mechanical Engineers (1972) presents correlations relating the orifice differential pressure to the flow rate for flow measurement purposes. In the model, the flow rate is known and the differential pressure is to be predicted, in order to facilitate orifice selection. The relationships listed in this section hold for flange taps as used on the 1500 hp test block's three flow measurement stations.

First, the volume flow rate based on the conditions upstream of the orifice is given by

$$\dot{V} = \dot{m}_i v_i, \quad (3.17)$$

which is used elsewhere in the correlations. The orifice (diameter d) and pipe (diameter D_{pipe}) cross-sectional areas, respectively, are given by

$$A_d = \frac{\pi}{4} d^2 \quad (3.18)$$

and

$$A_D = \frac{\pi}{4} D_{\text{pipe}}^2. \quad (3.19)$$

Then the average velocity, \mathcal{V}_D , in the pipe is

$$\mathcal{V}_D = \dot{V} / A_D, \quad (3.20)$$

and the corresponding Reynolds number is

$$\text{Re}_{D,\text{pipe}} = \frac{\rho_i \mathcal{V}_D D_{\text{pipe}}}{\mu_i}. \quad (3.21)$$

The velocity and Reynolds number at the orifice can be calculated using the same equations but substituting d and A_d instead of D and A_D . Even though compressibility effects are present, it

is assumed that the pipe inlet properties can be used for calculations at the orifice location because the effect of compressibility on thermophysical properties will be small over the differential pressure across the orifice.

For convenience, PTC 19.5 also defines a ratio of diameters, $\beta = d/D_{\text{pipe}}$, which is used throughout the calculations. For flange taps, the correlations relating differential pressure to mass flow rate take a nested form. The orifice coefficient of discharge, C , is represented by

$$C = K \sqrt{1 - \beta^4}, \quad (3.22)$$

where the flow coefficient

$$K = K_0 \left(1 + \frac{\alpha}{\text{Re}_d} \right). \quad (3.23)$$

Here,

$$\alpha = d \left(830 \text{ in}^{-1} - (5000 \text{ in}^{-1})\beta + (9000 \text{ in}^{-1})\beta^2 - (4200 \text{ in}^{-1})\beta^3 + \frac{530 \text{ in}^{0.5}}{\sqrt{D}} \right) \quad (3.24)$$

and

$$K_0 = K_e \left(\frac{10^6 d}{10^6 d + (15 \text{ in})\alpha} \right). \quad (3.25)$$

The expression for K_e uses singularity function notation; that is, if the quantity in angle brackets is negative, then that term becomes zero.

$$K_e = 0.5993 + \frac{0.007 \text{ in}}{D} + \left(0.364 + \frac{0.076 \text{ in}^{0.5}}{\sqrt{D}} \right) \beta^4 + 0.4 \left(1.6 - \frac{1 \text{ in}}{D} \right)^5 \langle 0.07 + 0.5 \text{ in}/D - \beta \rangle^{5/2} \\ - \left(0.009 + \frac{0.034 \text{ in}}{D} \right) \langle 0.5 - \beta \rangle^{3/2} + \left(\frac{65 \text{ in}^2}{D^2} + 3 \right) \langle \beta - 0.7 \rangle^{5/2}. \quad (3.26)$$

To account for the compressibility of the refrigerant, PTC 19.5 defines the expansion factor,

$$Y = 1 - (0.41 + 0.35\beta^4) \frac{\Delta p}{p_i \gamma}, \quad (3.27)$$

where Δp is the orifice differential pressure, $p_i - p_o$, and γ is the ratio of specific heats evaluated at upstream conditions, $\gamma = c_p/c_v$. The model also has provisions for choked flow,

which may occur when running the orifice selection routine over large flow ranges with the smaller orifices. From Munson et al. (2009),

$$p_{o,\text{choked}} = p_i \left(\frac{2}{\gamma + 1} \right)^{\gamma/(\gamma-1)} ; \quad (3.28)$$

and if $p_{o,\text{choked}} > p_{o,\text{free}}$, where free denotes the un-choked outlet pressure, then the flow is said to be choked. The model selects the larger of the two pressures to continue calculations. Finally, the compressible orifice equation is used to relate the differential pressure to the mass flow rate:

$$\dot{m} = C Y A_d \sqrt{2\rho_i \Delta p}. \quad (3.29)$$

In addition to the pressure calculations, mass and energy balances are required for this single-input, single-output device:

$$\text{Mass:} \quad 0 = \dot{m}_i - \dot{m}_o \quad (3.30)$$

$$\text{Energy:} \quad 0 = \dot{Q} - \dot{W} + (\dot{m}h)_i - (\dot{m}h)_o. \quad (3.31)$$

The orifice is modeled as a rigid, well-insulated control volume with no shaft work. So $\dot{Q} = \dot{W} = 0$, and thus $h_o = h_i$ for the orifice.

3.4 Flow Split

The flow split is assumed to be rigid and well-insulated with a negligible pressure drop. Additionally, the two outlet states are modeled as being the same as the inlet state, so

$$T_o = T_{o,\text{HGBP}} = T_i \quad (3.32)$$

and

$$p_o = p_{o,\text{HGBP}} = p_i, \quad (3.33)$$

where subscript “o” indicates the main outlet flow stream (leading to the condenser) and subscript “o, HGBP” indicates the flow stream bypassing the condenser. The actual division of mass flow rate between the two outlets is determined elsewhere in the model, by requiring that the throttled condensed stream mix with the throttled hot gas bypass stream in the correct proportion to re-establish the specified compressor suction condition.

3.5 Condenser

The condenser has two flow streams: a refrigerant stream and a water stream. These streams are unmixed, so the mass balances for each stream are given by

$$\dot{m}_{r,i} = \dot{m}_{r,o} \quad (3.34)$$

and

$$\dot{m}_{w,i} = \dot{m}_{w,o}, \quad (3.35)$$

where \dot{m}_r and \dot{m}_w are used to simplify the notation for the refrigerant and water streams, respectively.

In the condenser, both the water and refrigerant streams are modeled as having constant pressure. The condenser is modeled as a rigid control volume with no shaft work so that $\dot{W} = 0$. It is also assumed to be well-insulated so that the heat transfer across the external boundary $\dot{Q} = 0$. The internal heat transfer is modeled using the NTU-effectiveness method derived by Incropera et al. (2007); this section contains the pertinent results.

For the condenser in the gas test block refrigeration cycle, the refrigerant is always the hot fluid and the water is always the cold fluid. Therefore, the heat capacities for the hot and cold flow streams are

$$C_h = \dot{m}_r c_{p,r} \quad (3.36)$$

and

$$C_c = \dot{m}_w c_{p,w}, \quad (3.37)$$

where the specific heats are evaluated at the inlet conditions of each flow stream. Although the specific heats vary slightly with temperature, the impact of assuming constant specific heats is negligible. In addition, evaluating specific heats at the inlet temperature greatly simplifies the

problem since the outlet temperatures are initially unknown. Then $C_{\min} = \min(C_b, C_c)$ and $C_{\max} = \max(C_b, C_c)$. The NTU for the condenser is defined by

$$\text{NTU} = \frac{UA}{C_{\min}}, \quad (3.38)$$

where UA is the overall heat transfer coefficient determined from experimental data.

In the NTU-effectiveness method, the heat transfer is modeled in terms of the effectiveness, ϵ , and the theoretical maximum heat transfer rate, \dot{Q}_{\max} , which represents the performance of heat exchanger with infinite surface area. The effectiveness is used to determine the actual heat transfer rate \dot{Q} , which is given by

$$\dot{Q} = \epsilon \dot{Q}_{\max}. \quad (3.39)$$

For a phase-change application such as the condensation process, the effectiveness ϵ is defined as

$$\epsilon = 1 - e^{-\text{NTU}}, \quad (3.40)$$

while the maximum theoretical heat transfer rate \dot{Q}_{\max} is calculated using

$$\dot{Q}_{\max} = \dot{m}_r (h_{r,i} - h_{r,T=T_{w,i}}), \quad (3.41)$$

which represents fully condensing and cooling the refrigerant stream to the inlet water temperature.

Finally, the enthalpies of the water and refrigerant exiting the condenser can be determined from an energy balance for each flow stream:

$$0 = -\dot{Q} + \dot{m}_r (h_{r,i} - h_{r,o}) \quad (3.42)$$

and

$$0 = \dot{Q} + \dot{m}_w (h_{w,i} - h_{w,o}). \quad (3.43)$$

Any other properties of the water and refrigerant exiting the condenser, such as temperatures, can be determined based on the known pressures and enthalpies.

3.6 Cooling Tower

The JCI gas test block has multiple rooftop cooling towers to reject energy from the cycle to the outdoor air. To simplify the model, these physical cooling towers are lumped into a single component. Additionally, experimental data for validation are only available on an overall basis and not for each individual tower. The aggregated cooling tower has two primary flow streams: a water stream requiring cooling and outdoor air, which is treated as a mixture of air and water vapor. These flow streams mix in the cooling tower and a portion of the water stream evaporates into the air-water vapor mixture. By convention, the mass balance for the air-water vapor mixture is written in terms of the dry air mass flow rates, which are equal for a steady-flow system:

$$\dot{m}_{a,i} = \dot{m}_{a,o}. \quad (3.44)$$

As in the condenser model, the notation \dot{m}_a will be used throughout for simplicity. For a mass balance on the water stream, an additional term, $\dot{m}_{w, \text{evap}}$, accounts for the water evaporated into the moist air stream, so the mass balance is

$$\dot{m}_{w,i} = \dot{m}_{w,o} + \dot{m}_{w, \text{evap}}, \quad (3.45)$$

where the water lost to evaporation is given by

$$\dot{m}_{w, \text{evap}} = \dot{m}_a (\omega_{a,o} - \omega_{a,i}). \quad (3.46)$$

In Eq. (3.46), $\omega_{a,o}$ and $\omega_{a,i}$ represent the absolute humidity ratio of the air-water vapor mixture at the cooling tower outlet and inlet, respectively.

Braun et al. (1989) developed correlations which are used to apply the NTU-effectiveness method to the cooling tower. First, the saturation specific heat, c_s , is approximated by

$$c_s = \frac{h_{a,s,i} - h_{a,s,o}}{T_{w,i} - T_{w,o}}, \quad (3.47)$$

where subscript s indicates that the enthalpy is to be evaluated for a saturated air-water vapor mixture. An effective mass flow rate, m^* , is defined as

$$m^* = \frac{\dot{m}_a}{\dot{m}_{w,i} c_{p,w} / c_s}, \quad (3.48)$$

where the water specific heat, $c_{p,w}$, is evaluated at the inlet conditions. The number of transfer units (NTU) for the cooling tower is calculated using a semi-empirical approach:

$$\text{NTU} = c \left(\frac{\dot{m}_{w,i}}{\dot{m}_{a,i}} \right)^{1+n}, \quad (3.49)$$

where c and n are empirically determined constants for the cooling tower. The cooling tower effectiveness, ϵ_a , is then defined as

$$\epsilon_a = \frac{1 - \exp(-\text{NTU}(1 - m^*))}{1 - m^* \exp(-\text{NTU}(1 - m^*))}. \quad (3.50)$$

Analogous to the energy balances for the condenser, the energy balance for the air-water vapor stream is

$$\dot{Q} = \epsilon_a \dot{Q}_{\max}, \quad (3.51)$$

where the maximum possible heat transfer, \dot{Q}_{\max} , is calculated by assuming that the outlet air is fully saturated at the inlet water temperature:

$$\dot{Q}_{\max} = \dot{m}_a (h_{a,s,T=T_{w,i}} - h_{a,i}). \quad (3.52)$$

The outlet air state is then calculated using

$$\dot{Q} = \dot{m}_a (h_{a,o} - h_{a,i}). \quad (3.53)$$

Finally, the outlet water temperature is given by

$$T_{w,o} = T_{w,i} - \frac{\dot{m}_{a,i} (h_{a,o} - h_{a,i})}{\dot{m}_{w,i} c_{p,w}}. \quad (3.54)$$

3.7 Expansion Devices

The actual gas test block cycle has a complicated arrangement of numerous valves and spray nozzles which simultaneously throttle and mix the condensed refrigerant stream with the bypassed refrigerant stream to reestablish the compressor suction conditions. For the purposes of a one-dimensional model, this complex arrangement may be separated into three distinct processes: throttling the condensed refrigerant stream to the cycle's low pressure (suction pressure), throttling the hot gas bypass refrigerant stream to the cycle's low pressure, and mixing the two refrigerant streams in the correct proportions to achieve the specified test suction conditions.

While the condensed refrigerant stream is a subcooled liquid or saturated liquid-vapor mixture and the hot gas bypass refrigerant stream is a superheated vapor, the theory for the throttling process is the same in both cases, as described in this section. The theory for the mixing process is described in Section 3.8.

The throttle is modeled as a rigid control volume with no shaft work ($\dot{W} = 0$). Additionally, it is assumed to be well-insulated ($\dot{Q} = 0$). The mass balance for this single input, single output system is

$$\dot{m}_i = \dot{m}_o. \quad (3.55)$$

The energy balance then reduces to

$$h_i = h_o. \quad (3.56)$$

The pressure at the exit of each throttle is assumed to be the compressor suction pressure, and thus the outlet states of the throttling devices are fixed by the known enthalpy and pressure.

3.8 Mixing Chamber

The mixing chamber also is assumed to be a rigid control volume which is well-insulated. It has two input streams (condensed and bypassed refrigerant) and one outlet

leading to the compressor suction inlet. The mass balance for the mixing chamber is

$$\dot{m}_i + \dot{m}_{i,\text{HGBP}} = \dot{m}_o. \quad (3.57)$$

The energy balance is given by

$$\dot{m}_i h_i + \dot{m}_{i,\text{HGBP}} h_{i,\text{HGBP}} = \dot{m}_o h_o. \quad (3.58)$$

It is assumed that the mixing process occurs at a constant pressure. Therefore, the two balances on the mixing chamber constrain the division of flow between the condensed and bypassed streams by requiring that their mixing re-establishes the specified suction condition.

CHAPTER 4

SOLUTION METHODOLOGY

The equations developed in Chapter 3 are implemented in Engineering Equation Solver (EES). This software package provides thermophysical property data, unit checking, a graphical user interface (GUI) framework, and an automatic equation blocking scheme for iteratively solving systems of simultaneous equations. These features, along with JCI compressor and test engineers' familiarity with the program, make EES an ideal choice for implementation of the gas test block model.

The model is implemented using an EES module for each device in the cycle. As much as possible, the equations and assumptions for each device are contained within the corresponding module. This facilitates a code structure analogous to the physical system and will simplify code maintenance for future modifications or improvements to the model. The overall structure of the implementation is described in Section 4.1.

One of the goals of the project is to provide a tool for selecting the best flow measurement orifice for conducting tests over a user-input range of operating points. Achieving this goal requires running the model with each orifice configuration at multiple operating points within the user-specified range of conditions. Because the EES software restricts the number of variables that can be stored, it is not feasible to store the properties at each point in the cycle for multiple operating points. However, in some situations, the user would like to know detailed information about the gas test block at a single operating point. For this reason, two EES programs were developed, each sharing a common code base but providing different outputs.

The first program computes results for the entire cycle, but only for a single operating point at a time. This program is used to evaluate the feasibility of achieving the desired test conditions under specified outdoor air conditions. If the cooling towers cannot transfer sufficient heat to fully condense the refrigerant, then the gas test block cannot operate at steady state. This model is discussed in more detail in Section 4.2. The second program has the

capability to evaluate and store orifice and compressor model results for multiple operating points. It calls only the compressor and orifice modules of the code to minimize the number of variables required. This model is used for orifice selection and is discussed in Section 4.3.

4.1 Implementation Structure

As discussed in the opening of Chapter 4, the code is organized in a way that mimics the physical connection of the devices in the cycle. Wherever possible, the balance equations, related assumptions, and any required correlations are placed into an EES module. The inputs of these modules represent the thermodynamic states of physical flow streams entering the device, and the outputs represent the states of the flow streams exiting the component. This makes the calling structure intuitive and allows for improvements in the modeling assumptions for a given component without disrupting the rest of the model.

The complete EES code is displayed and briefly explained in Appendix A. The modules do not refer to state numbers (from, for example, Fig. 1.2) so that additional components can be added in the future with minimal disruption. Only the indices of the top-level array variables, such as the pressure and temperature arrays, correspond to the state numbering. This code is used as the basis for both the complete cycle program and the orifice selection program. Each of these programs uses the diagram window functionality of EES to provide a user interface for the model.

4.2 Complete Cycle Program

The diagram window for the complete cycle program is shown in Fig. 4.1. The required inputs are grouped into three clusters: the outdoor air conditions at the upper left, the block configuration settings (including orifice index as listed in Table 4.1) at the upper right, and the compressor operating point parameters to the left of the compressor. The compressor suction conditions are specified just below the compressor on the diagram.

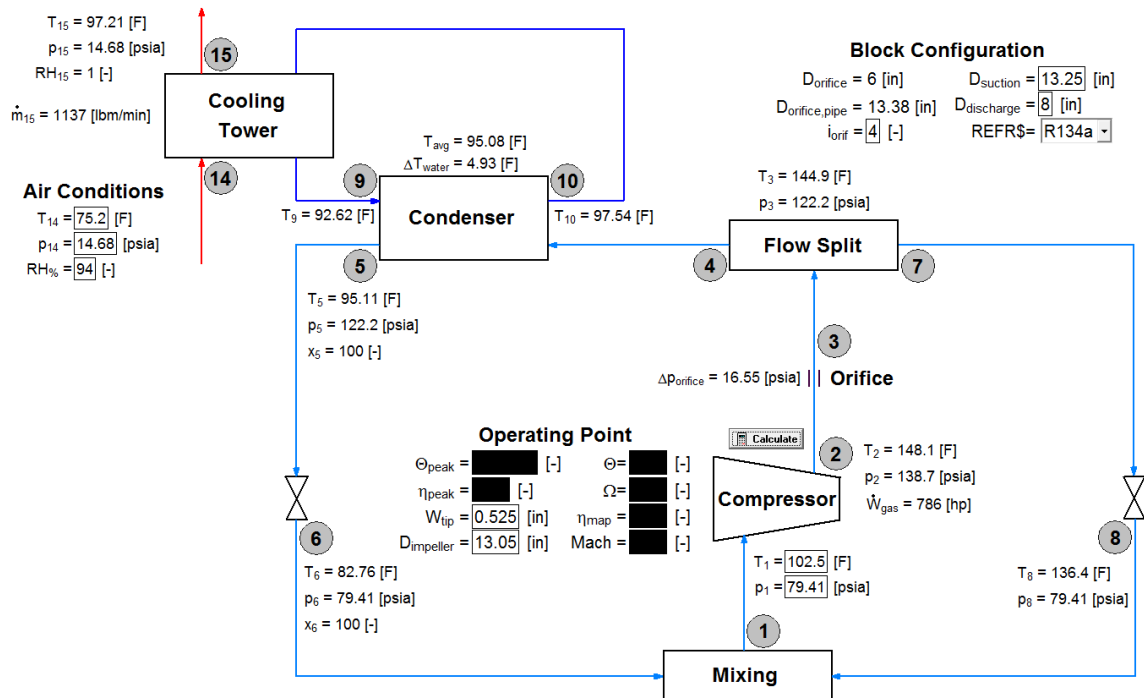


Figure 4.1: Engineering Equation Solver (EES) Diagram Window for the complete cycle program. User inputs are boxed numbers, while program outputs are displayed without boxes.

After specifying the inputs, the program may be run using the ‘Calculate’ button. The updated output states and other calculated values, such as compressor power, are displayed near the corresponding state point on the diagram. These results and additional outputs, such as enthalpies, may also be viewed using the results windows, which are organized by module, and the arrays window. In addition, the model may be run directly from the Equations Window or from a Parametric Table to study multiple operating conditions. If the calculated air mass flow rate through the model cooling tower exceeds the nominal air flow rate for the cooling towers on the gas test block, the specified operating condition is predicted to be infeasible at the given outdoor air conditions.

4.3 Orifice Selection Program

The orifice selection program calls only the compressor and orifice modules of the main code, which are the only modules required to model the orifice differential pressure. In order to

Table 4.1: Orifice numbering and diameter data for the modeled test block (Graham, 2006). This table corresponds to the information stored in the EES lookup table ‘OrificeData’.

Orifice	d (in)	D_{pipe} (in)
1	10.032	13.375
2	9.000	13.375
3	7.499	13.375
4	6.000	13.375
5	3.256	13.375
6	2.505	13.375
7	4.125	6.065
8	3.502	6.065
9	2.751	6.065
10	1.551	6.065
11	2.063	3.068
12	1.749	3.068
13	1.356	3.068
14	0.7815	3.068

obtain accurate mass flow measurements, the orifice differential pressure must be within the range 10 inH₂O to 990 inH₂O (Trevino, 2012). Therefore, it can be used to evaluate the suitability of different flow measurement orifices over a specified range of test conditions. Simplifying the model to only two modules keeps the orifice selection program within the maximum number of variables allowed by EES. A flowchart of the orifice selection algorithm is shown in Fig. 4.2.

Initially, the compressor module is called once to establish the discharge conditions based on suction conditions and compressor map parameters. Next, beginning with the minimum flow coefficient, Θ_{min} , specified by the user, the orifice differential pressure is evaluated and stored for each possible combination of orifice diameter and pipe diameter. These diameters are stored in an EES lookup table, which allows for straightforward modification as required in the future. The orifice numbering scheme and orifice data are shown in Table 4.1. The flow coefficient is then increased by $\Delta\Theta$ and this calculation process is repeated for each flow coefficient in the range $\Theta_{\text{min}} \leq \Theta \leq \Theta_{\text{max}}$.

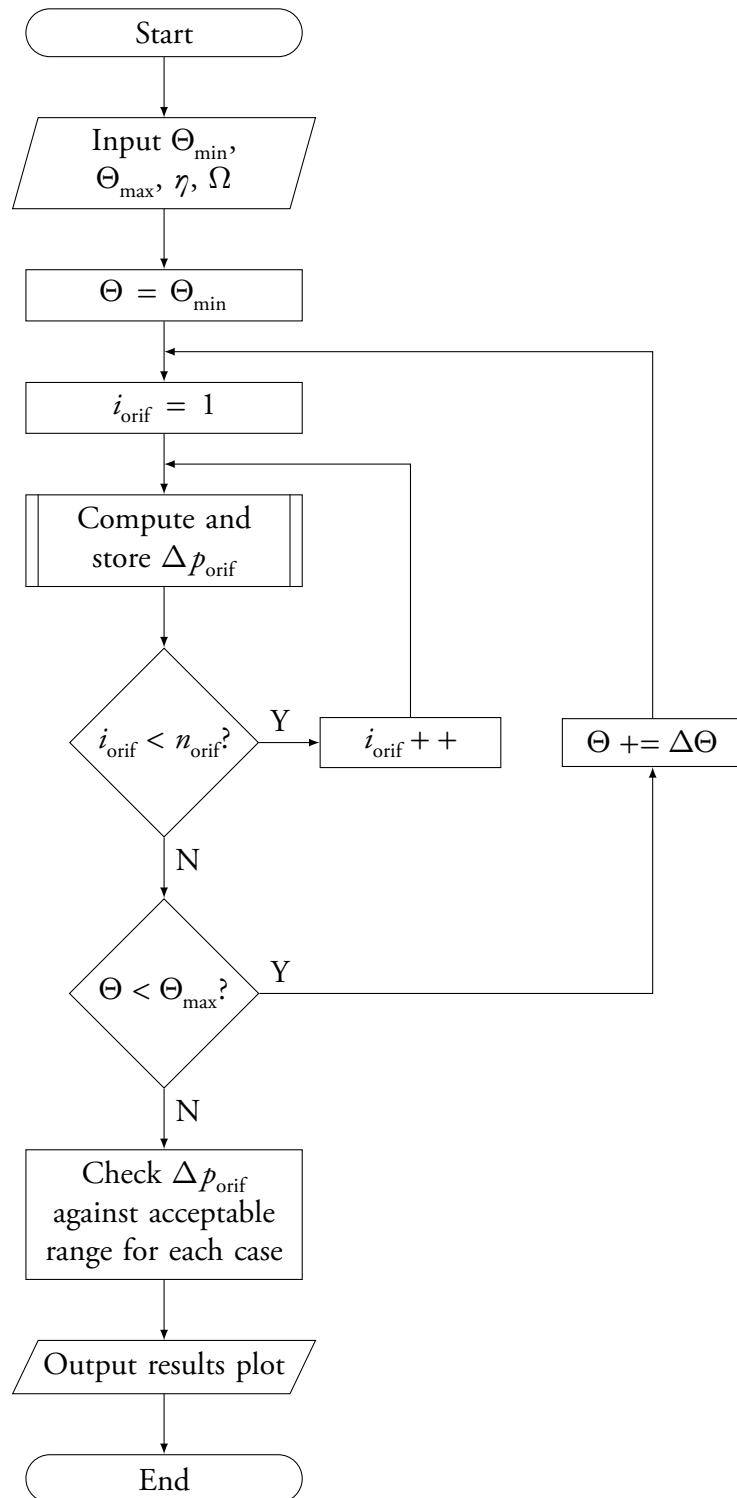


Figure 4.2: Flowchart for orifice selection procedure. The inner loop is over the orifices listed in Table 4.1 and the outer loop is over the user-specified range of flow coefficients.

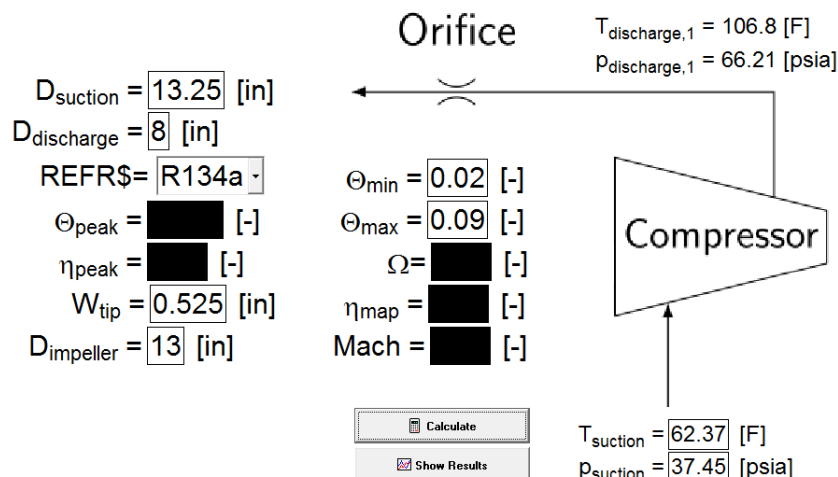


Figure 4.3: Engineering Equation Solver (EES) Diagram Window for the orifice selection program. User inputs are boxed numbers, while program outputs are displayed without boxes.

The diagram window for the orifice selection program is shown in Fig. 4.3. The number of flow coefficients evaluated within the user-specified range is set in the equations window so that the program does not exceed the maximum number of variables allowed by EES. If, for some reason, this limit is exceeded, an error message will appear with a statement to that effect. Proper operation is restored by selecting ‘Options’ → ‘Purge Unused Variables’ and selecting ‘Yes’ in the dialog box that appears. The model uses a uniform step size, $\Delta\Theta$, to determine the conditions to be evaluated within the user-specified range of flow coefficients.

The EES model generates a plot illustrating the differential pressure for each orifice over the specified range of flow conditions. The results are plotted on semi-logarithmic axes for clarity at both high and low differential pressures. A typical set of results is shown in Fig. 4.4. The ordinate axis limits correspond to the acceptable differential pressure range for flow measurement, 10 inH₂O to 990 inH₂O, or 0.36 psid to 35.70 psid. Therefore, a particular orifice is acceptable only if its differential pressure curve remains within the axis limits over the desired range of flow coefficients.

As discussed in Section 3.3, the model considers the possibility of choked flow through the orifices by comparing the predicted differential pressure to the maximum differential

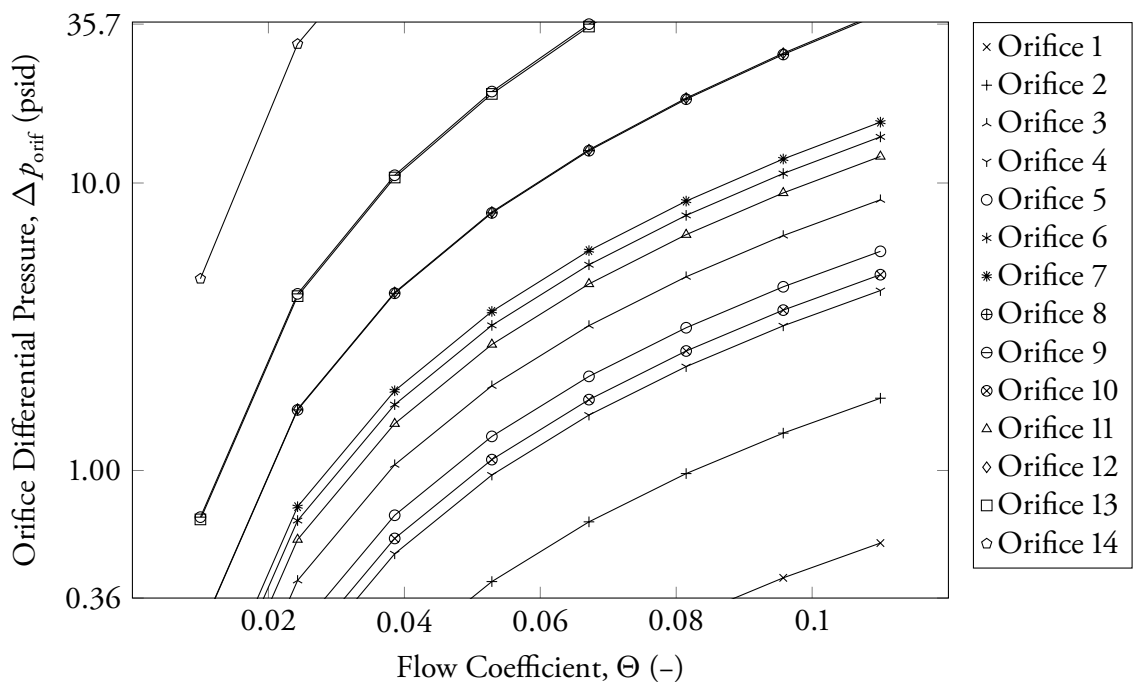


Figure 4.4: Typical orifice selection program results. The axis limits correspond to the 10 inH₂O to 990 inH₂O acceptable measurement range.

pressure, which occurs with choked flow. If choked flow is predicted, it will limit the mass flow rate, and thus the specified operating point cannot be achieved on the gas test block with the specified orifice. Sample results for choked flow are shown in Fig. 4.5. For this scenario, orifices 1 and 2 do not reach choked conditions, while orifices 3–14 experience choked flow and reach the maximum differential pressure. In this case, only orifice 2 would be acceptable, since orifice 1 does not provide the necessary differential pressure at the low end of the range of flow coefficients.

Figures 4.4 and 4.5 illustrate how the model output will enable JCI engineers to quickly select appropriate orifices for compressor testing. In addition, the outputs of the complete cycle program (Section 4.2) allow JCI engineers to determine if a test condition is feasible at the specified outdoor air conditions. Chapter 5 discusses the methods used to validate both programs, and shows that the model outputs achieve sufficient agreement with experimental data from the 1500 hp gas test block.

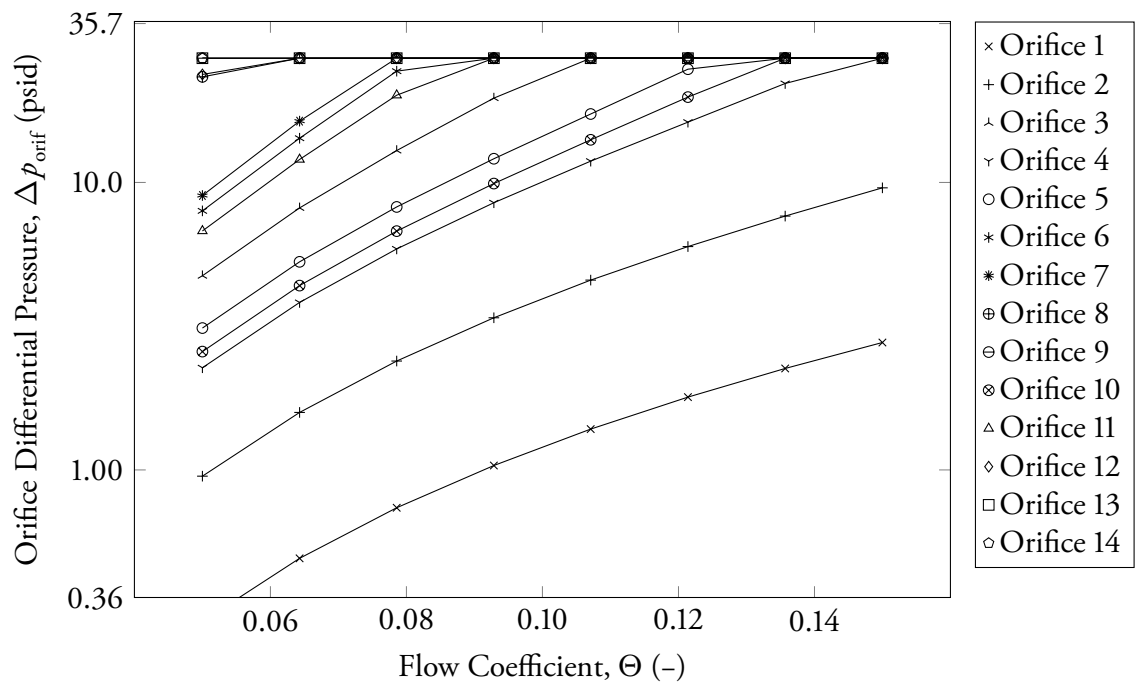


Figure 4.5: Orifice selection program results showing choked flow for orifices 3–14. For these conditions, only orifice 2 is acceptable over the entire range of flow coefficients.

CHAPTER 5

RESULTS AND DISCUSSION

A crucial component of any modeling effort is to confirm that the model agrees with experimental data to a level appropriate for the intended application. This validation process confirms the appropriateness of the simplifying assumptions made during the model development. For the 1500 hp gas test block, experimental data are available for numerous tests conducted in July 2005 and November 2012. The test data from JCI were obtained using the guidelines in Graham (2006) and in accordance with Gerber (1998), as described in Section 2.1.1. A subset of the test data used for validation purposes is shown in Table B.1 of Appendix B.

The complete cycle model was run with inputs matching each experimental data set to validate the model over a wide range of operating conditions. Because outdoor air conditions were not recorded at the time of the test, the conditions have been sourced from weather data archives (Weather Underground, Inc., 2005, 2012). The resulting model output variables are compared with the experimental data in Section 5.1. Parity plots are used to illustrate the agreement between the model results and experimental data. The results agree to within 2.5% in the compressor and orifice modules, and to within 2.0% in the condenser and cooling tower modules, which required broader assumptions.

Section 5.2 studies the effect of intermediate variables on the overall results. For example, subtle differences between the calculation methods used in the model and used during experiments mean that the Reynolds numbers for the compressor and the orifice do not agree with the experimental data nearly as well as other variables. However, while the Reynolds numbers have a subtle effect on the compressor discharge state and the orifice differential pressure, the sensitivity analysis reveals that the overall results are not significantly affected. Therefore, the sensitivity analysis is an essential step in proving the robustness of the model.

5.1 Comparison of Experimental and Model Results

This section presents the validation results for the complete cycle program. A sample set of detailed results is shown in Table B.1. Based on the data collected by JCI during each test, the compressor, orifice, and condenser module results from the model may be directly compared to experimental data. The results for each condition considered are summarized in parity plots, Figs. 5.1 to 5.9, alongside related discussion. Each parity plot illustrates perfect agreement between modeled and experimental results with a solid line and $\pm 5\%$ difference bounds with dashed lines, unless otherwise noted.

5.1.1 Compressor Module

Because the compressor module is based on compressor characteristics that are determined through experimental testing, the results are expected to show excellent agreement. Indeed, the maximum percent difference for the compressor discharge pressure is 0.018%, as shown in Fig. 5.1. Similarly, the maximum difference for the compressor discharge temperature (Fig. 5.2) is 1.0 °F, or 0.2% by using an absolute temperature scale. The error is still acceptable in this case, but is larger because of a difference in the compressor Reynolds number computation.

The undetermined difference in calculation methods results in an average of 12% difference between the compressor Reynolds number calculated in the model and calculated during experiments, as shown in Fig. 5.3. This impacts the Reynolds number correction (Eq. (3.11)) used in the calculation of isentropic efficiency. Because the model predicts a larger Reynolds number than was calculated during experiments, the model also will predict a greater isentropic efficiency. Therefore, the model will tend to slightly underpredict the discharge temperature, as seen in Fig. 5.2. The sensitivity of the model to this Reynolds number and its impact on model outputs is studied further in Section 5.2.

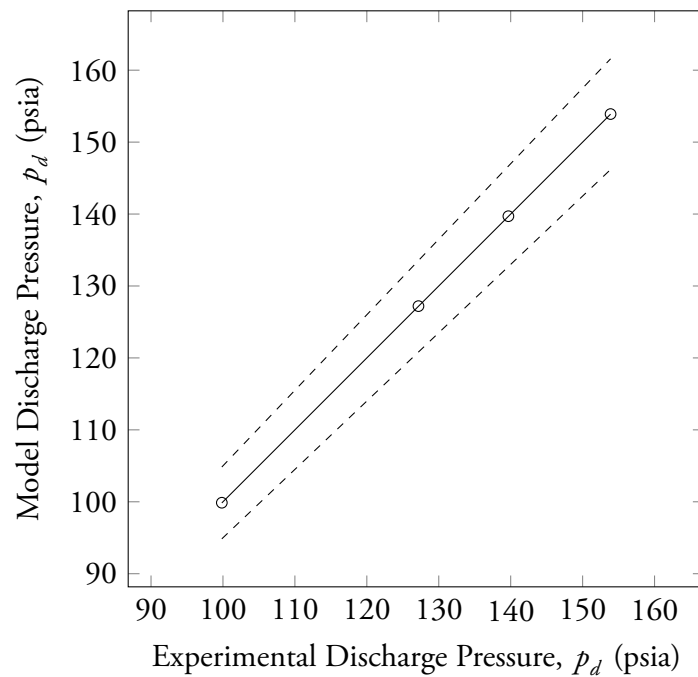


Figure 5.1: Compressor discharge pressure parity plot.

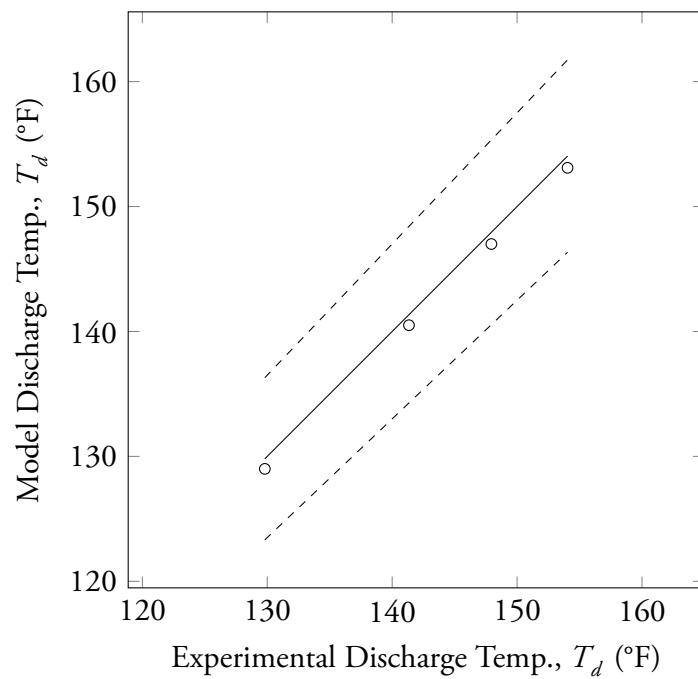


Figure 5.2: Compressor discharge temperature parity plot.

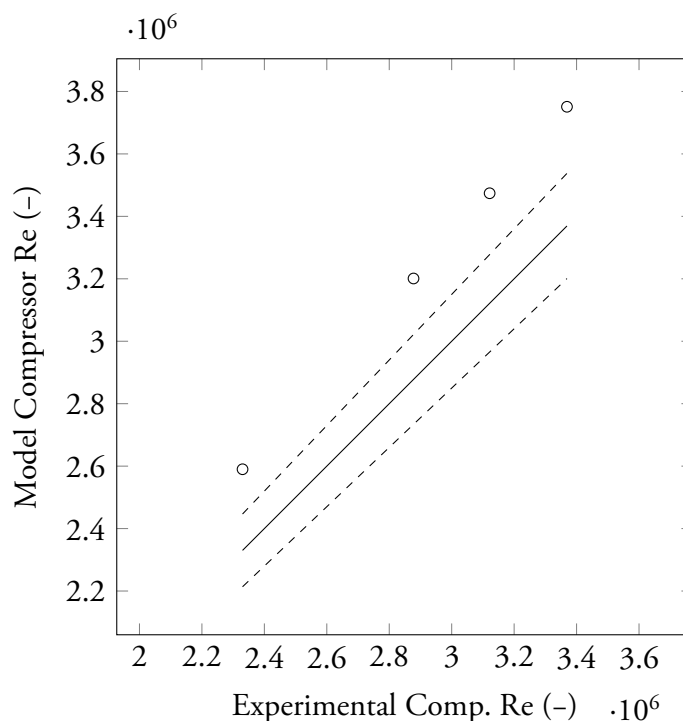


Figure 5.3: Compressor Reynolds number parity plot.

The compressor gas horsepower is shown in Fig. 5.4. This required output of the model agrees with the experimental results to within 2.5%. The compressor Reynolds number calculation affects the gas horsepower slightly, because the lower discharge temperature predicted by the model corresponds to a lower discharge enthalpy, and the gas horsepower is directly proportional to the increase in enthalpy across the compressor (Eq. (3.15)). Another possible source of error is the assumption of an adiabatic compressor. Heat transfer from the compressor casing to the ambient environment would increase the gas horsepower requirement for the test block.

5.1.2 Orifice Module

While the temperature at the orifice has only a slight effect on the differential pressure correlations (Section 3.3), there is a significant length of refrigerant piping between the orifice flow meter and the compressor discharge port. Therefore, comparing the model's predicted

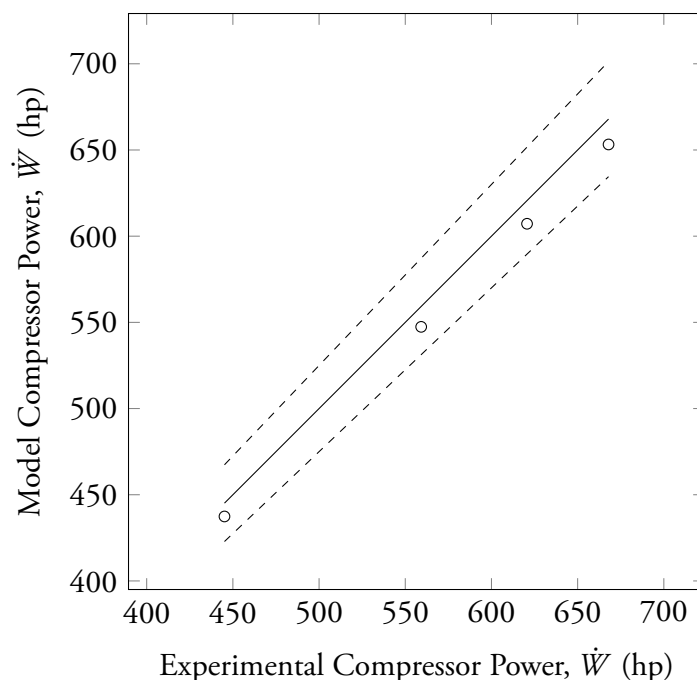


Figure 5.4: Compressor gas horsepower parity plot.

orifice temperature to the measured data provides a means to evaluate the assumption of negligible heat transfer from piping on the test block. The results for orifice temperature have a maximum difference of 2 °F or 0.5% on an absolute temperature scale, as shown in Fig. 5.5. Because the model consistently predicts a higher temperature than was measured, it is expected that heat transfer to the ambient environment is the cause of this difference. However, the orifice differential pressure (Fig. 5.6) is the important output in this area of the model. The impact of this temperature difference on the differential pressure is negligible, so the assumption is deemed appropriate.

The orifice differential pressure is the primary output of the model in the orifice selection program. The differential pressure is used to evaluate the suitability of different orifice diameters for the range of test conditions specified. As shown in Fig. 5.6, the model shows excellent agreement with the experimental results, with a maximum percent difference of 0.35% for the conditions considered for validation. This shows that the orifice selection program will be an excellent aid to simplify the calculations required to plan a set of tests.

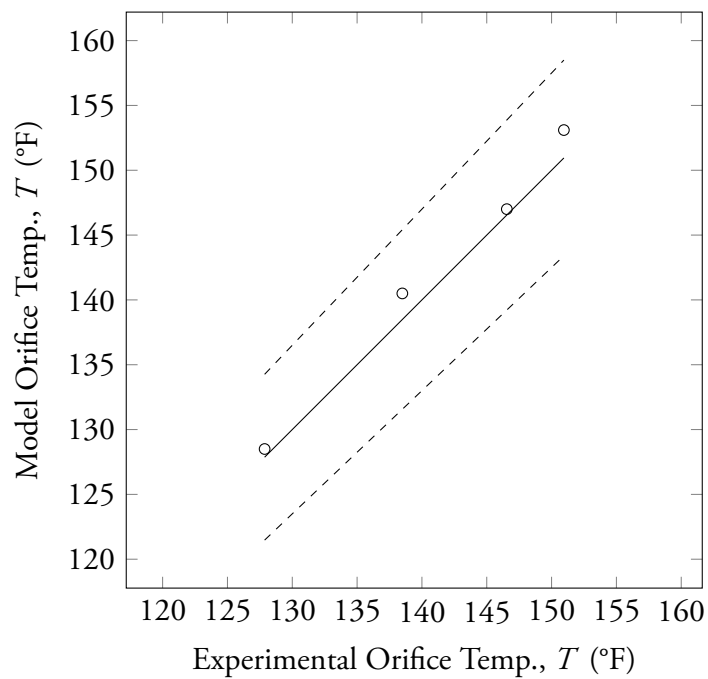


Figure 5.5: Orifice temperature parity plot.

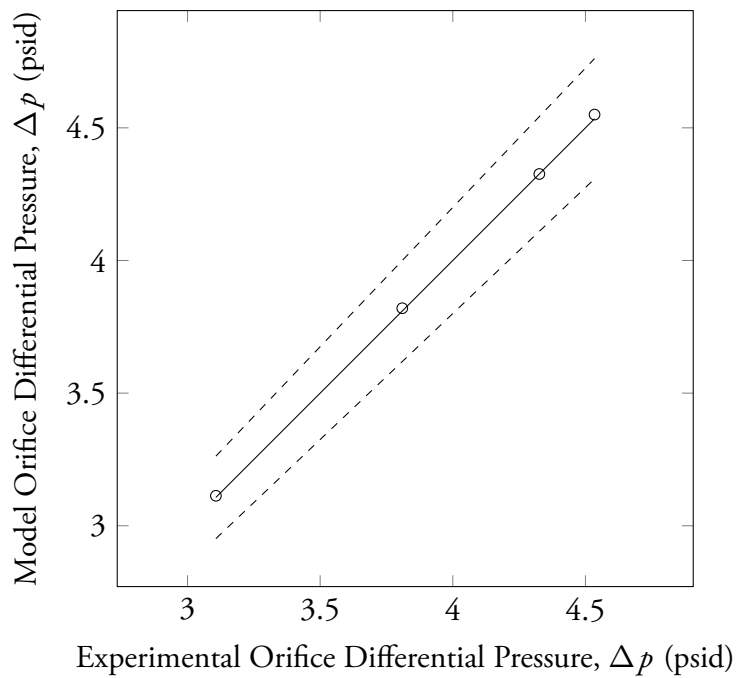


Figure 5.6: Orifice differential pressure parity plot.

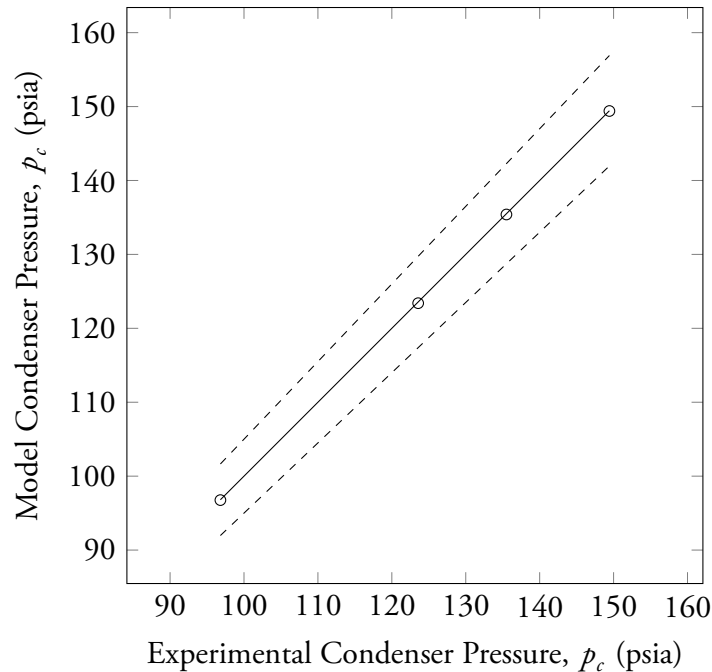


Figure 5.7: Condenser pressure parity plot.

5.1.3 Condenser Module

In the condenser, the outlet pressure is recorded in the experimental data. This allows the constant pressure assumptions in the flow split (Section 3.4) and condenser (Section 3.5) modules to be evaluated. As shown in Fig. 5.7, the model results for condenser pressure deviate from the experimental results by a maximum of 0.15%. Therefore, the constant pressure assumptions in the components and connecting piping are reasonable for the 1500 hp gas test block.

The condenser refrigerant liquid temperature is also recorded, and it can be used to calculate the degree of subcooling in the condenser. The comparison of modeled and measured liquid temperature is used to confirm that the condenser model provides an accurate representation of the complex heat transfer taking place. Figure 5.8 shows the results for the condenser refrigerant liquid temperature, which have a maximum deviation from experimental results of 1.5 °F or 0.5% on an absolute temperature scale.

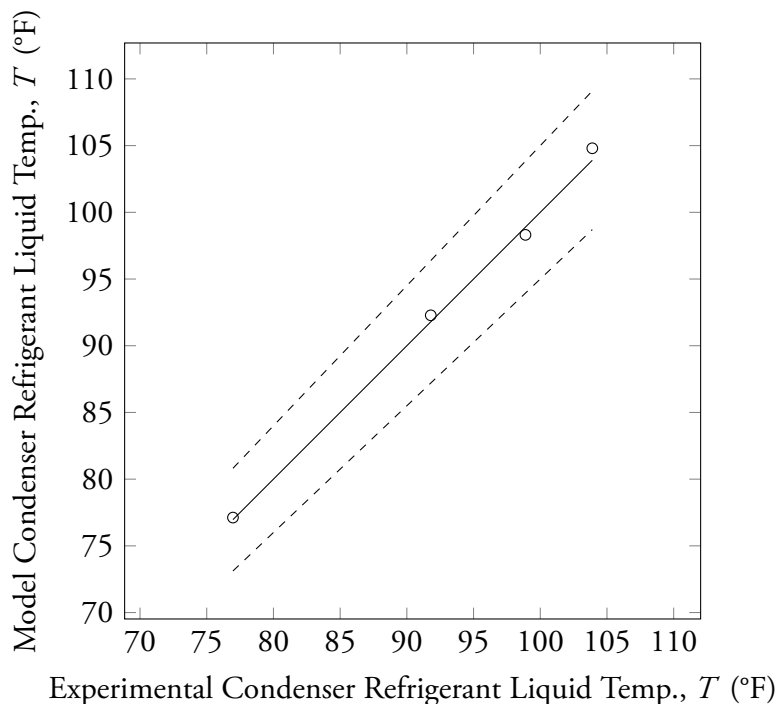


Figure 5.8: Condenser refrigerant liquid temperature parity plot.

5.1.4 Cooling Tower Module

The average condenser water temperature, which is also the average water temperature in the cooling tower, provides insight into the performance of both the cooling tower and condenser. Figure 5.9 shows a comparison of model and experimental results. Despite many assumptions concerning the parameters used in the condenser and cooling tower models, such as UA , c , and n (Sections 3.5 and 3.6), the results agree with the experimental data to within 5 °F or 2% on an absolute temperature scale.

Because the parameters are currently empirically-based, these differences are liable to increase at operating conditions further away from the conditions recorded in the experimental data. Recall from Section 3.6 that several cooling towers on the physical test block are lumped into a single cooling tower for the purposes of the model. In addition, neither the cooling tower fan speeds nor the condenser water flow rate are recorded as part of the test data, so average values are currently used. This is discussed further in Section 5.2, and several of the

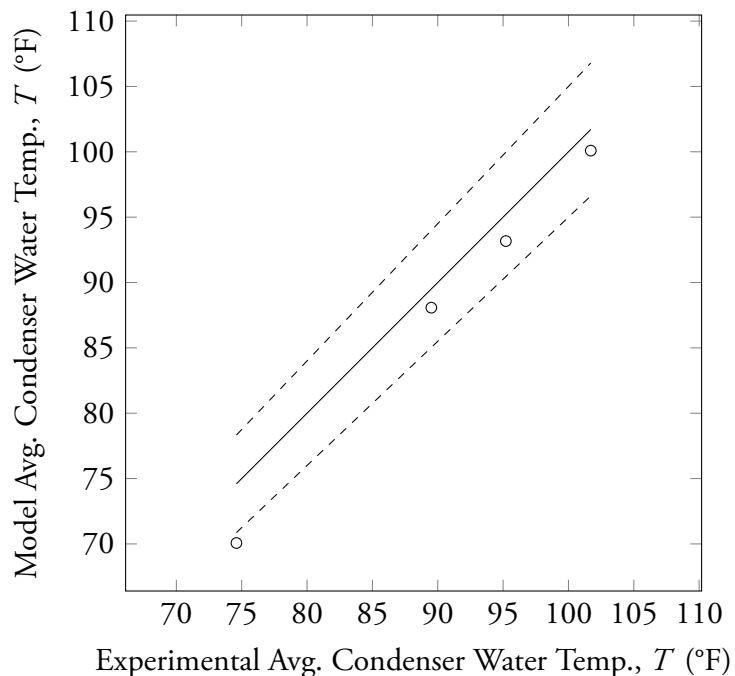


Figure 5.9: Average condenser water temperature parity plot.

recommendations discussed in Chapter 6 directly relate to additional data collection in these areas of the test facility. These improvements would lead to enhanced parameter selection in this area of the model.

5.2 Sensitivity Analysis

This section shows that the differences between Reynolds numbers calculated in the compressor and orifice modules (Sections 5.1.1 and 5.1.2) and calculated based on experiments have a negligible impact on the important output variables. It also studies the impact of the condenser water flow rate on the water temperatures and cooling tower flow rate requirements, because of the uncertainty involved in estimating the water flow rate. The model currently uses an average water flow rate calculated from test data. This is because a bypass loop is used on the block, but no data on the bypass loop flow rate or condenser loop flow rate are currently recorded.

Table 5.1: Sensitivity analysis results for the compressor Reynolds number, Re . The reference Reynolds number for this condition is $Re = 2.591 \times 10^6$.

Adjustment factor for calculated Re	Discharge pressure, p_d (psia)	Discharge temperature, T_d (°F)	Gas horsepower, \dot{W}_{gas} (hp)
0.85	99.87	129.2	438.7
0.90	99.87	129.1	438.2
0.95	99.87	129.0	437.8
1.00	99.87	129.0	437.4
1.05	99.87	129.0	437.1
1.10	99.87	129.0	436.7
1.15	99.87	128.9	436.4

In the compressor, the Reynolds number is used in the calculation of the isentropic efficiency, which affects the discharge temperature and thus the gas horsepower of the compressor. The discharge pressure should not be affected. To study the extent of these effects, the Reynolds number was artificially adjusted by several different percentages, and the compressor module outputs were recorded. These results are listed in Table 5.1. As expected, the discharge pressure is not affected. The discharge temperature is affected by a maximum of 0.2 °F, while the gas horsepower is affected by a maximum of 1.3 hp. These results show that the effect of the Reynolds number discrepancy on the outputs is very slight. Therefore, the error in the compressor gas horsepower (Fig. 5.4) is mostly attributable to the adiabatic assumption of Section 3.2.

The Reynolds number calculated at the orifice shows the same discrepancy as the calculation at the compressor. In the orifice, the Reynolds number has a slight effect on the coefficient of discharge, C , calculated using the ASME PTC 19.5 correlations (American Society of Mechanical Engineers, 1972) of Section 3.3. The orifice Reynolds number was adjusted to study the significance of these effects. The effects on the orifice module are even less significant than the effects on the compressor module. Table 5.2 displays the results, and it is clear that the effect is well under the level of uncertainty in the measurements

Table 5.2: Sensitivity analysis results for the orifice Reynolds number, Re . The reference Reynolds number for this condition is $Re = 7.891 \times 10^6$.

Adjustment factor for calculated Re	Outlet temperature, T_o (°F)	Orifice differential pressure, Δp_{orif} (psid)
0.85	128.37291	3.11289
0.90	128.37290	3.11294
0.95	128.37289	3.11298
1.00	128.37288	3.11303
1.05	128.37288	3.11306
1.10	128.37287	3.11310
1.15	128.37286	3.11313

on the gas test block. Therefore, the discrepancy in Reynolds number calculation is clearly negligible for the orifice module.

In the condenser, an average water flow rate calculated using experimental results is used in the absence of true flow rate measurements. The distribution of water flow between the condenser loop and the bypass loop is unknown. Changes in the water flow rate will affect the water temperatures at the condenser and, most importantly, the required air mass flow rate in the cooling tower. Table 5.3 shows the effects of changing the condenser water flow rate on the condenser water temperature difference, average water temperature, and also the cooling tower air mass flow rate. For a 30% change in water flow rate, the cooling tower air flow rate changes by only 3%. The water temperatures are affected slightly, but overall, the cooling tower mass flow rate is fairly insensitive to the specified condenser water mass flow rate.

Table 5.3: Sensitivity analysis results for the condenser water mass flow rate, \dot{m}_w . The reference water flow rate for this condition is $\dot{m}_w = 6768 \text{ lbm min}^{-1}$.

Adjustment factor for flow rate \dot{m}_w	Water temperature difference, ΔT_w (°F)	Average water temperature, T_{avg} (°F)	Cooling tower air flow rate, \dot{m}_a (lbm min ⁻¹)
0.85	3.227	70.38	917.4
0.90	3.048	70.29	923.0
0.95	2.888	70.21	928.3
1.00	2.743	70.14	933.1
1.05	2.613	70.07	937.6
1.10	2.494	70.02	941.7
1.15	2.385	69.96	945.6

CHAPTER 6

CONCLUSIONS AND RECOMMENDATIONS

This chapter contains a summary of the research work presented in this thesis and discusses the resulting conclusions. In addition, it contains recommendations for future improvements to the model and test block data acquisition. These data acquisition improvements would enable more extensive validation of the model, which in turn would improve the accuracy of the model by guiding the selection of empirical parameters.

The motivations and requirements described in Chapter 1 guided the development of a thermodynamic model of the 1500 hp hot gas bypass test block facility located in York, PA. After presenting prior research in Chapter 2, the simplifying assumptions used in developing the model were outlined in Chapter 3. These simplified equations were numerically solved by implementation in EES as discussed in Chapter 4. Graphical interfaces were presented for the two main use cases of the model: the complete cycle simulation and the orifice selection program.

Chapter 5 showed the results of the validation effort in which model outputs were compared to experimental data from the test block. These results showed that the model is accurate enough for the intended application and that the assumptions applied in developing the equations are appropriate. Sensitivity analyses conducted on several parameters in the model showed that even when intermediate results do not fully agree with experimental data, the primary outputs remain sufficiently accurate.

6.1 Conclusions

Based on the results presented and discussed in Chapter 5, the model meets the two primary goals of predicting whether test conditions are feasible and assisting in orifice selection. These goals were accomplished by predicting the air mass flow rate in the cooling tower and predicting the differential pressure across the orifice. If the predicted air mass flow rate exceeds the capacity of the cooling towers, then it is likely that the specified test condition is infeasible

at the given outdoor air conditions. Similarly, the orifice differential pressure must fall within a specified range in order to be suitable for measuring the refrigerant mass flow rate. Therefore, the orifice selection program allows engineers to specify a desired range of test conditions and then displays the orifice differential pressure for a number of operating points within the specified range. This allows the engineer to make an informed decision about the best orifice for the test plan without tedious calculations.

For the validation cases of Chapter 5, the maximum percent difference between model and experimental results is 2.5%, indicating that the model is quite accurate given the number of assumptions involved. The model's prediction of cooling tower air flow rate cannot be assessed because it is not measured during tests, but the primary output variable for orifice selection, the orifice differential pressure, agrees with the experimental results to within 0.35%. It should be noted, however, that the validation encompassed only a small range of test points and weather conditions, from which several of the parameters in the model are defined. Results for operating conditions far removed from the validation data may vary. Methods for correcting this shortcoming of the model are discussed in Section 6.2.

6.2 Recommendations

As noted in Chapter 5 and Section 6.1, the condenser and cooling tower modules of the model make significant assumptions to determine the parameters that characterize their performance. These parameters include the overall heat transfer coefficient for the condenser, UA , and the two characteristic parameters for the cooling tower model's calculation of NTU, c and n . Calculating these parameters using first principles was not a central focus of this project, because they are affected by many complex transport processes. Instead, these parameters were defined empirically, using average values calculated over the validation data sets. For this reason, the model results may not be as accurate for test conditions far removed from the validation test conditions. To improve these portions of the model, a number of data collection recommendations are prudent.

First, the cooling tower fan speeds should be recorded as part of each test. Currently, the fan speeds are adjusted until the test block reaches steady state at the desired operating point. Combined with fan curves for the cooling towers installed on the block, records of the fan speeds will allow calculation of the cooling tower model parameters c and n . This will enhance the accuracy of the cooling tower model and extend the range of test conditions over which its accuracy is acceptable. At the present time, the model uses typical values for these parameters from Braun et al. (1989).

Similarly, a means to determine the condenser water flow rate would greatly improve the accuracy of calculations for the condenser overall heat transfer coefficient, UA . As discussed in Section 5.2, the condenser water pump drives the flow through both a bypass loop and the condenser loop. With the current instrumentation setup, the division of flow between these loops is unknown. If the condenser water flow rate is known, then a more reliable estimate of UA could be produced.

Other potential improvements to the model concern the adiabatic and constant pressure assumptions. It is shown in Section 5.1.3 that the constant pressure assumption is valid for the sizes of pipe used on the gas test block. Additionally, the adiabatic assumption is shown to be valid for the orifice in Section 5.1.2. However, the adiabatic assumption for the compressor results in underprediction of the compressor gas horsepower, as discussed in Section 5.1.1. A model of the heat transfer from the compressor casing to the ambient conditions is likely to improve this prediction. Only the compressor module and the overall energy balance for the cycle would need to be modified to implement this improvement.

Because of the modular construction of the model, it will be relatively straightforward to implement any of these improvements. The data collection additions on the gas test block may prove more difficult to complete, but if these are possible, they would expand the validation possibilities and allow for better estimation of the characteristic parameters in the model. In addition, the model serves its intended purpose as it currently stands. Therefore, it is expected that the thermodynamic model will serve as a useful tool for conducting efficient compressor tests at the 1500 hp gas test block facility.

BIBLIOGRAPHY

- American Society of Mechanical Engineers. (1972, January). *ASME PTC 19.5-1972: Flow Measurement*. The American Society of Mechanical Engineers. New York.
- Aurora Pentair Water. (2007, March). *6 × 8 × 15 Series 410 Enclosed Impeller Pump Curves* (Technical catalog No. 410). Retrieved March 24, 2014, from <http://files.pentairliterature.com/MergedPDFs/201432475718.pdf>
- Baltimore Aircoil Company, Inc. (2001, July 18). *B.A.C. Cooling Tower Selection Program: Selection Parameters*.
- Braun, J. E., Klein, S., & Mitchell, J. (1989). Effectiveness models for cooling towers and cooling coils. *ASHRAE Transactions*, *95*, 164–174.
- Çengel, Y. A. & Boles, M. A. (2011). *Thermodynamics: An Engineering Approach* (7th ed.). New York: McGraw Hill.
- Dirlea, R., Hannay, J., & Lebrun, J. (1996). Testing of refrigeration compressors without condensation. In *Proceedings of international compressor engineering conference at purdue university* (1113, pp. 241–246). University of Liège. Belgium. Retrieved March 24, 2014, from <http://docs.lib.purdue.edu/icec/1113/>
- Gerber, G. J. (1998, September 30). *ASME PTC 10-1997: Performance Test Code on Compressors and Exhausters*. The American Society of Mechanical Engineers. New York.
- Graham, E. (2006, February 13). *Operating limits, 1500 hp compressor test facility, test facility #104, building 10* (Technical Report No. EF-104-06). York International Corporation.
- Iancu, F. V. (2012, April 23). *One-dimensional model of a closed loop refrigeration test block for compressors*. Johnson Controls, Inc.
- Incropera, F. P. & DeWitt, D. P. (1985). *Fundamentals of heat and mass transfer* (2nd ed.). New York: John Wiley and Sons, Inc.
- Incropera, F. P., DeWitt, D. P., Bergman, T. L., & Lavine, A. S. (2007). *Introduction to heat transfer* (5th ed.). Hoboken, NJ: John Wiley and Sons, Inc.
- J.N.O. (1983, December 16). *Condenser-Freon-12, 36 in O.D. × 12 ft L.G., 2-pass finned tube*. Engineering Drawing EF-104-66D.

- J.N.O. (1984, March 27). *Flow Diagram: 1500 hp Turbo Compressor Test Facility, Building 10*. Engineering Drawing EF-104-2D.
- Kauffman, J. P. & Sommer, S. T. (2006, October 9). *Reynolds Correction Logic—Compressor Efficiency Correction*. Johnson Controls, Inc.
- Kays, W. & London, A. (1984). *Compact heat exchangers* (3rd ed.). New York: McGraw-Hill.
- McGovern, J. (1984). Analysis of a refrigerant compressor load stand incorporating hot gas bypass and a single full condensation heat exchanger. In *Proceedings of the international compressor engineering conference at purdue university* (491, pp. 468–477). Trinity College. Dublin, Ireland.
- Mitchell, J. W. & Braun, J. E. (2013). *Principles of heating, ventilation, and air conditioning in buildings*. Hoboken, NJ: John Wiley and Sons, Inc.
- Munson, B., Young, D., Okiishi, T., & Huebsch, W. (2009). *Fundamentals of fluid mechanics* (6th ed.). Hoboken, NJ: Wiley.
- Qureshi, B. A. & Zubair, S. M. (2006, March 9). A complete model of wet cooling towers with fouling in fills. *Applied Thermal Engineering*, 26, 1982–1989.
- Sahs, L. J. & Mould, H. W., Jr. (1956, February 7). *Apparatus for testing refrigeration compressors*. 2733600. Buffalo, NY.
- Sommer, S. T. (2013, July 22). Personal Communication.
- Trevino, J., Jr. (2012, November 16). Personal Communication.
- Weather Underground, Inc. (2005, July 25). Weather history for york, pa | weather underground. Retrieved March 28, 2014, from http://www.wunderground.com/history/airport/KTHV/2005/7/25/DailyHistory.html?req_city=NA&req_state=NA&req_statename=NA&MR=1
- Weather Underground, Inc. (2012, November 16). Weather history for york, pa | weather underground. Retrieved March 28, 2014, from http://www.wunderground.com/history/airport/KTHV/2012/11/16/DailyHistory.html?req_city=NA&req_state=NA&req_statename=NA
- Wilcox, E. (2007, August). Performance testing guidelines for centrifugal compressors. *Hydrocarbon Processing*, 59–69.
- York Division, Borg-Warner Corporation. (n.d.). *Horizontal Shell and Tube Condenser, Water Cooled, Refrigerants-12, 22, and 502: Form 195.11-TM*.

APPENDIX A

ENGINEERING EQUATION SOLVER (EES) CODE LISTING

This appendix lists the complete EES code for the thermodynamic model of the test block. The main EES code is displayed in Listing A.1. This section allows the user to specify the operating parameters of the desired test and calls additional modules (Listings A.4 to A.9) which contain the bulk of the equations in the model.

Listing A.1: Main EES program code.

```

1 "1D Compressor Test Block Model"
2 "Author: Paul Gessler"
3 "Marquette University"
4
5 "MODULES INSERTED HERE"
6
7 "Reference State"
8 $REFERENCE R134a DFT
9
10 "Constants"
11 g_c = 32.174*Convert(lbm-ft/lbf-s^2, lbm-ft/lbf-min^2)
12
13 "Data Conversions (for convenience)"
14 RH[14] = RH_%/100
15 W_dot_gas = -W_dot_12*Convert(Btu/min, hp)
16
17 "Setup Orifice"
18 D_orifice = LOOKUP('OrificeData', i_orif, 'D_orifice')
19 D_orifice_pipe = LOOKUP('OrificeData', i_orif, 'D_orifice_pipe')
20
21 "Default Settings for Running without Diagram"
22 $IFNOT DiagramWindow
23     "Test Operating Parameters"
24     p[1] = 37.4548 [psia]
25     T[1] = 62.37 [F]
26     eta_map = "JCI PROPRIETARY"
27     eta_peak = "JCI PROPRIETARY"
28     THETA_peak = "JCI PROPRIETARY"
29     THETA = "JCI PROPRIETARY"
30     OMEGA = "JCI PROPRIETARY"
31     Mach = "JCI PROPRIETARY"
32

```

```

33     "Test Block Configuration Parameters"
34     REFR$ = 'r134a'
35     D_impeller = 13 [in]
36     W_tip = 0.431 [in]
37     i_orif = 4 [-]
38     D_suction = 12 [in]
39     D_discharge = 8 [in]
40
41     "Outdoor Air Conditions"
42     T[14] = 55 [F]
43     p[14] = 14.7 [psia]
44     RH_% = 70 [-]
45 $ENDIF
46
47 "Condenser Water Conditions"
48 m_dot[9] = 6768 [lbm/min] "based on calculattions from 2012 data"
49
50 x[1] = Quality(REFR$, T=T[1], p=p[1])
51 CALL Compressor(REFR$, D_impeller*Convert(in, ft), W_tip*Convert(in, ft),
    D_suction*Convert(in,ft), D_discharge*Convert(in,ft), g_c, THETA, OMEGA,
    Mach, eta_map, eta_peak, THETA_peak, p[1], T[1], x[1] : p[2], T[2], x[2],
    m_dot[1], m_dot[2], W_dot_12)
52
53 CALL Orifice(REFR$, g_c, D_orifice*Convert(in, ft), D_orifice_pipe*Convert(in,
    ft), T[2], p[2], x[2], m_dot[2] : T[3], p[3], x[3], m_dot[3], DELTAp_orifice
    )
54
55 CALL FlowSplit(T[3], p[3], x[3] : T[7], p[7], x[7], T[4], p[4], x[4])
56
57 CALL Condenser(REFR$, T[4], p[4], x[4], T[9], p[9], m_dot[9], W_dot_12 : T[5], p
    [5], x[5], m_dot[5], T[10], p[10], m_dot[10], m_dot[4])
58 DELTAT_water = T[10] - T[9]
59 T_avg = (T[10]+T[9])/2
60
61 p[6] = p[1]
62 CALL Throttle(REFR$, T[5], p[5], x[5], m_dot[5], p[6] : T[6], x[6], m_dot[6])
63
64 p[8] = p[1]
65 CALL Throttle(REFR$, T[7], p[7], x[7], m_dot[7], p[8] : T[8], x[8], m_dot[8])
66
67 m_dot[1] = m_dot[6] + m_dot[8]
68
69 {CALL MixingChamber(m_dot[1] : m_dot[8], m_dot[6])}
70
71 CALL CoolingTower(T[10], p[10], m_dot[10], T[14], RH[14], p[14], -W_dot_12 : T
    [11], p[11], m_dot[11], T[15], RH[15], p[15], m_dot[15], m_dot[14])

```

```

72 m_dot[14] = Density(AIRH2O, T=T[14], p=p[14], R=RH[14])*V_dot_air
73
74 "Close condenser water loop"
75 T[9] = T[14] + (T[4] - T[14])/4
76 p[9] = 14.7 [psia]
77
78 "Output variables for plotting"
79 h[1] = MyEnthalpy(REFR$, T[1], p[1], x[1])
80 h[2] = MyEnthalpy(REFR$, T[2], p[2], x[2])
81 h[3] = MyEnthalpy(REFR$, T[3], p[3], x[3])
82 h[4] = MyEnthalpy(REFR$, T[4], p[4], x[4])
83 h[5] = MyEnthalpy(REFR$, T[5], p[5], x[5])
84 h[6] = MyEnthalpy(REFR$, T[6], p[6], x[6])
85 h[7] = MyEnthalpy(REFR$, T[7], p[7], x[7])
86 h[8] = MyEnthalpy(REFR$, T[8], p[8], x[8])
87
88 s[1] = MyEntropy(REFR$, T[1], p[1], x[1])
89 s[2] = MyEntropy(REFR$, T[2], p[2], x[2])
90 s[3] = MyEntropy(REFR$, T[3], p[3], x[3])
91 s[4] = MyEntropy(REFR$, T[4], p[4], x[4])
92 s[5] = MyEntropy(REFR$, T[5], p[5], x[5])
93 s[6] = MyEntropy(REFR$, T[6], p[6], x[6])
94 s[7] = MyEntropy(REFR$, T[7], p[7], x[7])
95 s[8] = MyEntropy(REFR$, T[8], p[8], x[8])

```

Alternatively, the user can specify the test parameters and view the model predictions in the *Diagram Window* as discussed in Chapter 4. One diagram window (Fig. 4.1) is for the complete cycle program, while the other (Fig. 4.3) is for the orifice selection program.

Many of the modules use several helper functions for common calculations. These include calculations of entropy and enthalpy for an arbitrary state point defined by temperature, pressure, and quality. The EES conventions of $x = 100$ for a superheated vapor and $x = -100$ for a subcooled liquid are used in these functions. A function is also provided for calculation of the Reynolds number. These functions are shown in Listing A.2.

Listing A.2: General helper functions.

```

1 FUNCTION MyEnthalpy(FLUID$, T, p, x)
2     "Returns enthalpy of an arbitrary state"
3     IF ((x>1) OR (x<0)) THEN MyEnthalpy := Enthalpy(FLUID$, T=T, p=p) ELSE
        MyEnthalpy := Enthalpy(FLUID$, T=T, x=x)

```

```

4 END
5
6 FUNCTION MyEntropy(FLUID$, T, p, x)
7     "Returns entropy of an arbitrary state"
8     IF ((x>1) OR (x<0)) THEN MyEntropy := Entropy(FLUID$, T=T, p=p) ELSE
9         MyEntropy := Entropy(FLUID$, T=T, x=x)
10
11 END
12
13 FUNCTION GetRe(rho, V, L, mu,g_c)
14     "Returns Reynolds number"
15     GetRe := rho*V*L/mu/g_c
16 END

```

The compressor and orifice modules use additional helper functions. The compressor module uses helper function GetX to calculate the flow ratio, X , as defined in Eq. (3.12) for the Reynolds number correction. The orifice uses a function K_e to compute the coefficient for the orifice correlations Eq. (3.26), as well as a function GetOrificePressure to determine if free or choked flow is applicable Eq. (3.28). These are displayed in Listing A.3.

Listing A.3: Helper functions specific to the compressor and orifice modules.

```

1 "COMPRESSOR HELPER FUNCTION"
2 FUNCTION GetX(THETA,THETA_peak)
3     "Returns flow ratio X"
4     X = THETA/THETA_peak
5     IF (X<1) THEN GetX := X ELSE GetX := 1
6 END
7
8 "ORIFICE HELPER FUNCTIONS"
9 FUNCTION K_e(D_pipe, beta)
10     "Returns K_e per ASME PTC 19.5 72"
11     K_e := 0.5993 + 0.007 [in]/D_pipe + (0.364 + 0.076 [in]^(0.5)]/sqrt(
12         D_pipe))*beta^4
13     IF (0.07 + 0.5 [in]/D_pipe > beta) THEN K_e := K_e + 0.4*(1.6 - 1 [in]/
14         D_pipe)^5*((0.07 + 0.5 [in]/D_pipe) - beta)^(5/2)
15     IF (beta < 0.5) THEN K_e := K_e - (0.009 + 0.034 [in]/D_pipe)*(0.5 -
16         beta)^(3/2)
17     IF (beta > 0.7) THEN K_e := K_e + (65 [in]^2)/D_pipe^2 + 3)*(beta - 0.7)
18         ^5/2)
19 END
20
21 FUNCTION GetOrificePressure(p_out_free, p_out_choked)

```

```

18     IF (p_out_choked > p_out_free) THEN GetOrificePressure := p_out_choked
19     ELSE GetOrificePressure := p_out_free
END

```

The remainder of the code consists of a MODULE for each device in the cycle. The assumptions and relationships developed in Chapter 3 are defined in these modules and applied to general balance equations. These modules are called by the main code of Listing A.1, and are shown in Listings A.4 to A.9.

The compressor module is displayed in Listing A.4.

Listing A.4: Compressor module of EES implementation.

```

1  MODULE Compressor(REFR$, D_impeller, W_tip, D_suction, D_discharge, g_c, THETA,
   OMEGA, Mach, eta_map, eta_peak, THETA_peak, p_suction, T_suction, x_suction
   : p_discharge, T_discharge, x_discharge, m_dot_suction, m_dot_discharge,
   W_dot_comp)
2     "get CFM and velocity for later calculations"
3     v_suction = Volume(REFR$, P=p_suction, T=T_suction)
4     CFM_compressor = m_dot_suction*v_suction
5     vel_suction = CFM_compressor/(PI*D_suction^2/4)
6
7     "perform Reynolds number correction"
8     X = GetX(THETA, THETA_peak)
9     rho_suction = Density(REFR$, T=T_suction, P=p_suction)
10    h_0_suction = h_suction + 0.5*vel_suction^2*Convert(ft^2/min^2,Btu/lbm)
11    T_t_suction = Temperature(REFR$, h=h_0_suction, P=p_suction)
12    p_t_suction = p_suction + 0.5*rho_suction*vel_suction^2*Convert(ft^-2,in
   ^-2)/g_c
13    mu_suction = Viscosity(REFR$, T=T_suction, P=p_suction)*Convert(lbm/ft-
   hr, lbf-min/ft^2)
14    Vel_tip = Mach*v_sound_suction
15    Re = GetRe(rho_suction, Vel_tip, W_tip, mu_suction, g_c)
16    eta_s = eta_map + X*((1 - eta_peak)*(1 - (10^6/Re)^(0.1)))
17
18    "dimensionless parameter definitions"
19    v_sound_suction = SoundSpeed(REFR$, T=T_suction, p=p_suction)*Convert(ft
   /s, ft/min) "calculate acoustic velocity"
20    THETA = CFM_compressor/(v_sound_suction*D_impeller^2)
21    OMEGA = g_c*(h_discharge_s - h_suction)*Convert(Btu, ft-lbf)/
   v_sound_suction^2
22    eta_s = (h_discharge_s - h_suction)/(h_discharge - h_suction)
23
24    "RPM check"

```

```

25     RPM = Vel_tip/(PI*D_impeller)
26
27     "state calculations"
28     T_sat_suction = Temperature(REFR$, P=p_suction, x=1.0)
29     DELTAT_sh = T_suction - T_sat_suction "compute degree of superheat (not
        currently used)"
30     h_suction = MyEnthalpy(REFR$, T_suction, p_suction, x_suction)
31     s_suction = Entropy(REFR$, P=p_suction, T=T_suction)
32     h_discharge_s = Enthalpy(REFR$, P=p_discharge, s=s_suction)
33     T_discharge = Temperature(REFR$, P=p_discharge, h=h_discharge)
34     x_discharge = Quality(REFR$, T=T_discharge, h=h_discharge)
35
36     "assumptions"
37     Q_dot_comp = 0 "assume well-insulated compressor"
38
39     "mass balance"
40     0 = m_dot_suction - m_dot_discharge "no leakage; steady flow; SIS0"
41
42     "energy balance"
43     0 = Q_dot_comp - W_dot_comp + m_dot_suction*h_suction - m_dot_discharge*
        h_discharge "steady flow; SIS0"
44 END

```

The orifice module is displayed in Listing A.5.

Listing A.5: Orifice module of EES implementation.

```

1  MODULE Orifice(REFR$, g_c, D_orifice, D_orifice_pipe, T_in, p_in, x_in, m_dot_in
    : T_out, p_out, x_out, m_dot_out, DELTAp_orifice)
2      "assumptions"
3      Q_dot_orifice = 0 "well-insulated"
4      W_dot_orifice = 0 "rigid CV; no shaft work"
5
6      "property lookups"
7      v_in = Volume(REFR$, P=p_in, T=T_in)
8      rho_in = Density(REFR$, P=p_in, T=T_in)
9      mu_in = Viscosity(REFR$, P=p_in, T=T_in)*Convert(lbm/ft-hr, lbf-min/ft
        ^2)
10
11     "Follows methodology used in ASME PTC 19.5 72"
12     V_dot_orifice = m_dot_in*v_in
13     A_0 = pi*D_orifice^2/4 "orifice throat area"
14     A_1 = pi*D_orifice_pipe^2/4 "orifice pipe area"
15     V_orifice_pipe = V_dot_orifice/A_1
16     V_orifice = V_dot_orifice/A_0

```

```

17 Re_orifice_pipe = GetRe(rho_in, V_orifice_pipe, D_orifice_pipe, mu_in,
    g_c)
18 Re_orifice = GetRe(rho_in, V_orifice, D_orifice, mu_in, g_c)
19 beta = D_orifice/D_orifice_pipe
20 C = K*sqrt(1 - beta^4)
21 K = K_0*(1 + A/Re_orifice)
22 K_e = K_e(D_orifice_pipe*Convert(ft, in), beta)
23 K_0 = K_e*(10^6*D_orifice*Convert(ft, in)/(10^6*D_orifice*Convert(ft, in)
    ) + 15 [in]*A))
24 A = D_orifice*Convert(ft, in)*(830 [in^(-1)] - 5000 [in^(-1)]*beta +
    9000 [in^(-1)]*beta^2 - 4200 [in^(-1)]*beta^3 + 530 [in^(-0.5)]/sqrt
    (D_orifice_pipe*Convert(ft, in)))
25 gamma = Cp(REFR$, T=T_in, p=p_in)/Cv(REFR$, T=T_in, p=p_in)
26 p_out_choked = p_in*(2/(gamma+1))^(gamma/(gamma-1))
27 Y = MIN(1, 1 - (0.41 + 0.35*beta^4)*((p_in - p_out_free)/p_in)/gamma) "
    expansion factor (for compressibility effects)"
28 p_out_free = MAX(p_out_choked, p_in - ((V_dot_orifice/(C*Y*A_0))^2)/(2*
    v_in*g_c*Convert(lbf/in^2, lbf/ft^2)/(1 - beta^4)))
29 p_out = GetOrificePressure(p_out_free, p_out_choked)
30 DELTAp_orifice = p_in - p_out
31
32 "mass balance"
33 0 = m_dot_in - m_dot_out "steady flow; SIS0"
34
35 "energy balance"
36 0 = Q_dot_orifice - W_dot_orifice + m_dot_in*h_in - m_dot_out*h_out "
    steady flow; SIS0"
37
38 h_in = MyEnthalpy(REFR$, T_in, p_in, x_in)
39 T_out = Temperature(REFR$, h=h_out, p=p_out)
40 x_out = Quality(REFR$, T=T_out, h=h_out)
41 END

```

The flow split module is displayed in Listing A.6.

Listing A.6: Flow split module of EES implementation.

```

1 MODULE FlowSplit(T_in, p_in, x_in : T_out_HGBP, p_out_HGBP, x_out_HGBP, T_out,
    p_out, x_out)
2     "assumptions"
3     {
4     Q_dot_FlowSplit = 0 [Btu/min] "well-insulated"
5     W_dot_FlowSplit = 0 [Btu/min] "rigid CV; no shaft work"
6     }
7     p_out = p_in
8     p_out_HGBP = p_out

```

```

9      {
10     h_out = h_in
11     h_out_HGBP = h_out
12     }
13     T_out = T_in
14     T_out_HGBP = T_out
15     x_out = x_in
16     x_out_HGBP = x_out
17
18     "property lookup"
19     {h_in = MyEnthalpy(REFR$, T_in, p_in, x_in)}
20
21     "mass balance"
22     {0 = m_dot_in - m_dot_out - m_dot_out_HGBP "steady flow; SIMO"}
23
24     "energy balance"
25     {0 = Q_dot_FlowSplit - W_dot_FlowSplit + h_in*m_dot_in - h_out*m_dot_out
      - h_out_HGBP*m_dot_out_HGBP "steady flow; SIMO"}
26 END

```

The condenser module is displayed in Listing A.7.

Listing A.7: Condenser module of EES implementation.

```

1  MODULE Condenser(REFR$, T_refr_in, p_refr_in, x_refr_in, T_water_in, p_water_in,
   m_dot_water_in, Q_dot_condenser : T_refr_out, p_refr_out, x_out,
   m_dot_refr_out, T_water_out, p_water_out, m_dot_water_out, m_dot_refr_in)
2     "assumptions"
3     W_dot_condenser = 0 [Btu/min] "rigid CV; no shaft work"
4     p_refr_out = p_refr_in "constant pressure -- shell side"
5     p_water_out = p_water_in "constant pressure -- tube side"
6     h_refr_out_guess = Enthalpy(REFR$, x=0.0, p = p_refr_out) "guess sat.
   liquid outlet"
7
8     "heat capacities"
9     C_c = m_dot_water_in*Cp(water, T=T_water_in, p=p_water_in)
10    C_h = m_dot_refr_in*Cp(REFR$, T=T_refr_in, p=p_refr_in)
11    C_min = MIN(C_c, C_h)
12    C_max = MAX(C_c, C_h)
13    {C_r = 0 "we have a condenser"}
14
15    "effectiveness-NTU relations"
16    NTU = 3 {UA/C_min} "eq. 11.24 of Incropera and DeWitt"
17    epsilon = 1 - exp(-NTU) "effectiveness; Table 11.3 Incropera and DeWitt"
18    Q_dot_max_1 = m_dot_refr_in*(h_refr_in - MyEnthalpy(REFR$, T_water_in,
   p_refr_out, -100))

```

```

19 Q_dot_max_2 = m_dot_water_in*(Enthalpy(water, T=Temperature(REFR$, p=
      p_refr_in, x=1.0), p=p_water_out) - h_water_in)
20 Q_dot_max = -Q_dot_max_1
21 Q_dot_condenser = epsilon*Q_dot_max "eq. 11.22 of Incropera and DeWitt (
      modified for phase-change)"
22
23 "property lookups"
24 h_refr_in = MyEnthalpy(REFR$, T_refr_in, p_refr_in, x_refr_in)
25 h_water_in = Enthalpy(water, T=T_water_in, p=p_water_in)
26 T_refr_out = Temperature(REFR$, h=h_refr_out, p=p_refr_out)
27 x_out = Quality(REFR$, p=p_refr_out, h=h_refr_out)
28 T_water_out = Temperature(water, h=h_water_out, p=p_water_out)
29
30 "mass balances"
31 0 = m_dot_refr_in - m_dot_refr_out "steady flow; unmixed streams"
32 0 = m_dot_water_in - m_dot_water_out "steady flow; unmixed streams"
33
34 "energy balances"
35 0 = Q_dot_condenser - W_dot_condenser + m_dot_refr_in*h_refr_in -
      m_dot_refr_out*h_refr_out "steady flow; unmixed streams"
36 0 = -Q_dot_condenser - W_dot_condenser + m_dot_water_in*h_water_in -
      m_dot_water_out*h_water_out "steady flow; unmixed streams"
37 END

```

The expansion device module is displayed in Listing A.8. This module is called for both the condensed stream and bypassed stream.

Listing A.8: Expansion device module of EES implementation.

```

1 MODULE Throttle(REFR$, T_in, p_in, x_in, m_dot_in, p_out : T_out, x_out,
      m_dot_out)
2     "assumptions"
3     Q_dot_throttle = 0 "well-insulated"
4     W_dot_throttle = 0 "rigid CV; no shaft work"
5
6     "mass balance"
7     0 = m_dot_in - m_dot_out "steady flow; SIS0"
8
9     "energy balance"
10    0 = Q_dot_throttle - W_dot_throttle + m_dot_in*h_in - m_dot_out*h_out "
      steady flow; SIS0"
11
12    "property lookups"
13    h_in = MyEnthalpy(REFR$, T_in, p_in, x_in)
14    T_out = Temperature(REFR$, h=h_out, p=p_out)

```

```

15     x_out = Quality(REFR$, h=h_out, p=p_out)
16 END

```

The cooling tower module is displayed in Listing A.9.

Listing A.9: Cooling tower module of EES implementation.

```

1  MODULE CoolingTower(T_water_in, p_water_in, m_dot_water_in, T_air_in, RH_air_in,
   p_air_in, Q_dot_tower : T_water_out, p_water_out, m_dot_water_out,
   T_air_out, RH_air_out, p_air_out, m_dot_air_out, m_dot_air_in)
2      "performance correlations"
3      c = 1.684 "typical value"
4      n = -0.391 "typical value"
5      NTU = c*(m_dot_water_in/m_dot_air_in)^(1 + n) "from Braun 1989"
6
7      "assumptions"
8      T_water_out_guess = WETBULB(AIRH2O, T=T_air_in, p=p_air_in, R=RH_air_in)
   "from Braun 1989"
9      p_water_out = p_water_in
10     p_air_out = p_air_in
11     m_dot_air_in = m_dot_air_out
12
13     "property lookups"
14     h_air_in = Enthalpy(AIRH2O, T=T_air_in, p=p_air_in, R=RH_air_in)
15     omega_air_in = HUMRAT(AIRH2O, T=T_air_in, p=p_air_in, R=RH_air_in)
16     h_water_sat_in = Enthalpy(AIRH2O, T=T_water_in, p=p_water_in, R=1)
17     c_p_water = Cp(WATER, T=T_water_in, p=p_water_in)
18
19     "effectiveness correlations"
20     c_s = (h_water_sat_in - h_water_sat_out)/(T_water_in - T_water_out) "
   from Braun 1989"
21     m|star = m_dot_air_in*c_s/(m_dot_water_in*c_p_water) "from Braun 1989"
22     epsilon_a = (1 - exp(-NTU*(1 - m|star)))/(1 - m|star*exp(-NTU*(1 - m|
   star)))
23
24     "from Braun 1989"
25     Q_dot_tower = epsilon_a*m_dot_air_in*(h_water_sat_in - h_air_in)
26     Q_dot_tower = m_dot_air_in*(h_air_out - h_air_in)
27     T_water_out = T_water_in - (m_dot_air_in*(h_air_out - h_air_in))/(
   m_dot_water_in*c_p_water)
28     h_water_sat_out = Enthalpy(AIRH2O, T=T_water_out, p=p_water_out, R=1)
29     m_dot_water_out = m_dot_water_in - m_dot_air_in*(omega_air_out -
   omega_air_in)
30     omega_air_out = HumRat(AIRH2O, h=h_air_out, p=p_water_out, R=RH_air_out)
31     T_air_out = Temperature(AIRH2O, h=h_air_out, p=p_water_out, R=RH_air_out)
32     RH_air_out = 1

```

```
33     {capacity = m_dot_water_in*c_p_water*range}
34     {range = T_water_in - T_water_out}
35     {approach = T_water_out - T_water_out_guess}
36 END
```

APPENDIX B

SAMPLE VALIDATION DATA AND RESULTS

Table B.1 shows sample validation results for a typical set of experimental data and corresponding model outputs. Information protected under intellectual property law has been removed from the table, replaced by 'JCI Proprietary'. Percent differences for temperatures are calculated using an absolute temperature scale.

Table B.1: Sample validation results. Protected information is removed from the table and denoted with 'JCI Proprietary'. Percent differences for temperatures are calculated on an absolute basis.

Parameter	Run Number:		18.00	
	Units	Actual	Model	% Diff.
Test Date	yyyy-mm-dd	2005-07-25	2005-07-25	INPUT
Test Time	hh:mm	22:45	22:45	INPUT
Outdoor Temperature	°F	75.20	75.20	INPUT
Barometric Pressure	psia	14.68	14.68	INPUT
Relative Humidity	%	94.00	94.00	INPUT
Compressor ID	–	H9	H9	INPUT
Refrigerant	–	134a	134a	INPUT
Tip Diameter, D	in	13.046	13.046	INPUT
Tip Width, b	in	0.525	0.525	INPUT
Suction Diameter	in	13.250	13.250	INPUT
Discharge Diameter	in	8.000	8.000	INPUT
Orifice Diameter	in	6.000	6.000	INPUT
Orifice Pipe Diameter	in	13.376	13.376	INPUT
Suction Pressure	psia	79.410	79.410	INPUT
Suction Temperature	°F	102.50	102.50	INPUT
Mach Number, Ma	–	JCI Proprietary		INPUT
Head Coefficient, Ω	–	JCI Proprietary		INPUT
Flow Coefficient, Θ	–	JCI Proprietary		INPUT
Efficiency, η_{map}	–	JCI Proprietary		INPUT
Discharge Pressure	psia	139.17	138.70	0.338
Discharge Temperature	°F	149.60	148.10	1.003
Compressor Reynolds Number	–	4.41×10^6	4.94×10^6	11.970
Gas Horsepower (Static)	hp	824.00	806.70	2.100
Orifice Temperature	°F	146.29	144.90	0.950
Orifice Differential Pressure	psid	16.65	16.55	0.601
Orifice Pressure	psia	137.46	138.70	0.902
Orifice Reynolds Number	–	1.76×10^7	2.00×10^7	13.750
Orifice Mass Flow Rate	lbm min ⁻¹	4296.70	4294.00	0.063
Condenser Pressure	psia	124.07	122.20	1.507
Cond. Refr. Liquid Temp.	°F	91.50	95.11	0.655
Condenser Water Out Temp.	°F	88.70	97.54	1.612
Condenser Water In Temp.	°F	86.58	92.62	1.106
Avg. Cond. Water Temp.	°F	87.64	95.08	1.359